VILNIUS UNIVERSITY
FACULTY OF CHEMISTRY AND GEOSCIENCES
INSTITUTE OF CHEMISTRY
DEPARTMENT OF APPLIED CHEMISTRY

Rugilė Žilėnaitė
Chemistry
Master thesis

SPECTROSCOPIC CHARACTERISATION OF NEW FLUORESCENT VISCOSITY SENSORS BASED ON BODIPY GROUP

Scientific advisor
dr. Aurimas Vyšniauskas

Scientific consultant
PhD student Karolina Maleckaitė

Vilnius 2022

TABLE OF CONTENT

LIST OF ABBREVIATIONS

^{13}C-dFT	^{13}C-labelled trityl spin probe
BODIPY	Boron-dipyrromethene/4,4-difluoro-4-bora-3a,4a-diaza-s-indacene
CCVJ	9-(2-carboxy-2-cyano)vinyl julolidine
DCM	Dichloromethane
DCVJ	9-(dicyanovinyl)-julolidine
DMSO	Dimethyl sulfoxide
DPH	1,6-diphenyl-l,3,5-hexatriene
EDG	Electron donating group
EPR	Electron paramagnetic resonance
EWG	Electron withdrawing group
FA	Fluorescence anisotropy
FCS	Fluorescence correlation spectroscopy
FLIM	Fluorescence lifetime imaging microscopy
FMR	Fluorescent molecular rotor
FRAP	Fluorescence recovery after photobleaching
GFP	Green fluorescent protein
GUV	Giant unilamellar vesicle
MEP	4-(methylamino)-2-ethyl-5,5-dimethyl-4-pyridine-2-yl-2,5-dihydro-1H-imidazol-1-oxyl
NADH	Nicotinamide adenine dinucleotide
NMR	Nuclear magnetic resonance
RNA	Ribonucleic acid
TCSPC	Time-correlated single-photon counting
TS	Transition state

INTRODUCTION

The microenvironment in the cell is defined by local viscosity, polarity (hydrophilicity/hydrophobicity), and temperature. Diffusion-controlled processes are ubiquitous and are extremely important within the cell; they play a crucial role in controlling the rate of mass transport and intercellular molecular interactions [1]. The rate of diffusion is closely related to the microviscosity of the surroundings. Atypical changes in microviscosity are associated with the development of various diseases and pathologies. In addition, temperature variations within the cell not only control thermodynamic processes but can also be a sign of infection or inflammation [2,3].

Well-known and developed tools, e.g., viscometer, thermometer, etc., are used to measure parameters in bulk, homogenous fluid. Unfortunately, the tools mentioned above are not useful on a microscale, e.g., a single cell, where the environment is heterogeneous [4]. Thus, it is necessary to have a tool for imaging of the microenvironment. One of the easiest methods to do that is by using viscosity-sensitive fluorophores, called fluorescent molecular rotors (FMRs). FMRs are the group of organic molecules, the luminescence of which depends on the viscosity of a medium [5].

Boron-dipyrromethene (BODIPY) based FMRs are widely used as viscosity sensors. Among them, BODIPY-C_{10} and other its derivatives are the most popular molecular rotors. Their main advantages are easy functionalisation, photostability, monoexponential fluorescence decay and relatively high molar extinction coefficient. However, their main drawback is absorption and fluorescence wavelengths. Most of the BODIPY based probes emit photons in a green spectral region, although while working with biological tissues, red or near-infrared light is more desirable [6,7].

The main focus of this work is to characterise new BODIPY-based fluorescent molecular rotors and assess how changes in the molecular structure influence their spectroscopic properties as well as sensitivity to the physical properties of a medium. To achieve this goal two main tasks were established:

1. Record absorption and fluorescence emission spectra as well as fluorescence decays to characterise the spectroscopic properties of the new BODIPY-based FMRs.
2. Investigate their dependences on the viscosity, polarity, and temperature of surrounding environment.

1. LITERATURE REVIEW

1.1 Microviscosity

Microviscosity can be defined as a friction experienced by a single molecule undergoing diffusion. Diffusion arises from a particle interaction with its environment at the microscale level. The strength of interactions increases with increasing fluid viscosity [8]. To better understand microviscosity, viscosity and diffusion must first be described and explained.

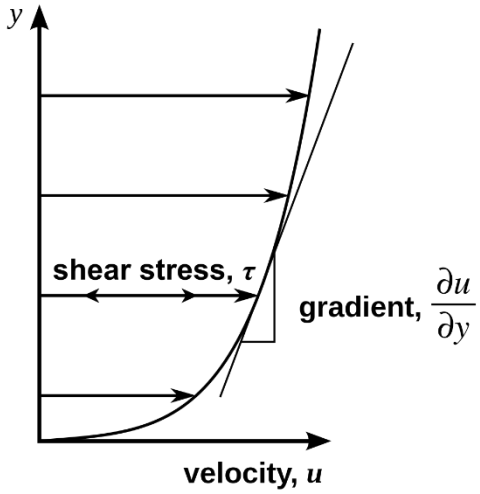

Fig. 1. *Schematic overview of shear stress in moving liquid layers* [9].

When explaining viscosity, it is useful to think of a fluid as separate flowing layers, with each layer moving at a different velocity. When two layers are moving relative to one another, and they are flowing at different velocities, a shear stress (τ) develops between them. The effect of shear stress has the biggest impact on a flow close to the wall. The velocity (u) of moving liquid layers that are in contact with the wall is zero. However, it increases with an increase in distance (y) to a wall (Fig. 1). The relationship between shear stress and the velocity gradient ($\partial u/\partial y$) is usually linear. Besides, the slope between them is the viscosity (η) [10]:

$$\tau = \eta \frac{\partial \mathrm{u}}{\partial \mathrm{y}}. \tag{1}$$

An alternative approach for defining viscosity is looking at the rotational movement of a particle in the fluid. If particle is defined as a sphere with radius (r), its translational (D_t) and rotational (D_r) diffusions are as follows [11]:

$$D_t = \frac{kT}{6\pi\eta r}, \tag{2}$$

$$D_r = \frac{kT}{8\pi\eta r^3} = \frac{kT}{6\eta V}, \tag{3}$$

where k – Boltzmann constant, T – absolute temperature, V – volume of the sphere. Two equations above link the diffusion coefficient and viscosity of the fluid together. Unfortunately, this connection is only valid while the rigid sphere is large enough compared to its surroundings. Difficulty arises

when system is shrunk from macroscopic to microscopic level, and term viscosity can no longer be used. When talking about microenvironment and microviscosity, other parameters should also be considered, e.g., size, shape, charge of the molecule, intermolecular interactions, etc. In addition, fluid cannot be assumed to be uniform and gaps in it (free volume) should be taken into consideration. In this approach, the movement of the molecule is characterised by two diffusional processes: movement of solvent molecules (Stokes diffusion) and migration into holes of the solvent (free volume diffusion) (Fig. 2) [8].

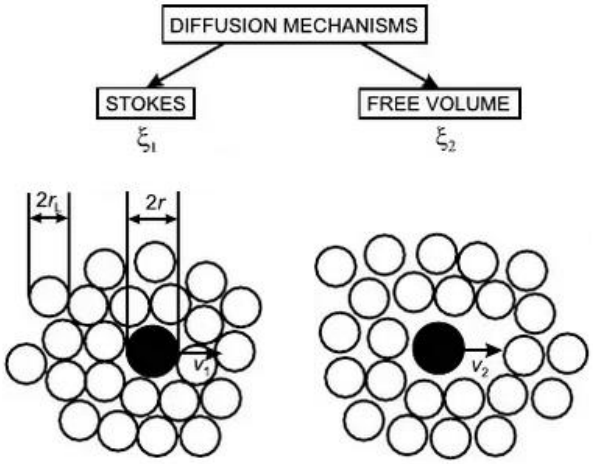

Fig. 2. *Stokes and free volume translational diffusion processes. Black circles – solute molecules, white circles – solvent molecules* [8].

Since on microscale level diffusion mechanism is different and molecule-fluid interactions must be considered, the term microviscosity is used instead of viscosity. Although microviscosity does not have an exact definition like its bulk counterpart viscosity, the importance of being able to measure it is significant. Viscosity is the paramount parameter and plays a significant role on the microscopic level in biosystems. It can determine the diffusion rate and various processes of the inner biological environment [5]. Cell membrane, cytoplasm, and other organelles have viscoelastic properties which can be influenced by external factors. Changes in intracellular microviscosity in a cell can occur during natural processes, although atypical changes are associated with the development of diseases or pathologies [12].

It was found out that an increase in red blood cell viscosity for people with diabetes is linked to the resistance to the insulin [13,14]. Another example is aesthosclerosis, during which arteries of patients become thicker and more rigid. Viscosity of the endothelial cell membrane increases, and accumulated cholesterol is involved in differences in nitric oxide synthase activity [15]. Moreover, patients with Alzheimer's disease have decreased platelet membrane viscosity [16]. Furthermore, the activity of ribonucleic acid (RNA), which is responsible for coding, regulation, expression of genes, etc., is extremely sensitive to the viscosity of living cells. Even slight changes can have an impact on RNA diffusion and movement rates. Disturbance of RNA functions can result in various cardiovascular and cerebrovascular illnesses [17]. All aforementioned examples show the importance of understanding and measuring microviscosity not only for the comprehension of diseases, but also for their diagnoses and treatment.

1.2 Microviscosity measurements

Bulk viscosity can be measured using conventional or in other words mechanical methods, i. e., rotational, the falling ball or capillary viscosimeter. Their working mechanism is based on determination of internal friction. Measurements usually last approximately 5 minutes and use relatively large volume of fluid. In addition, instruments require maintenance and cleaning after every sample. Besides, using mechanical methods real-time or localised measurements are not possible. Thus, measurements of microviscosity with conventional methods could be time-consuming and inaccurate because of unwanted biological sample interaction with instruments, e.g., protein adherence [12]. Usually, local microviscosity is measured using either spectroscopic or fluorescent methods.

1.2.1 Spectroscopic techniques

Among spectroscopic techniques, nuclear magnetic resonance (NMR) and electron paramagnetic resonance (EPR) are the two most used methods to sense viscosity on the microscale. The working principle of NMR is based on the spin quantum number. The spin quantum number is associated with the angular momentum of an electron. The spin quantum number can be either +½ or -½, where ½ is the magnitude, and +/- is the direction of the spin vector. Nuclei of an atom with either odd mass, odd atomic number or both has a quantised spin angular momentum. Only atoms which total spin number is not whole are registered in NMR spectra. In addition, nucleus is electrically charged, and, in the movement, it generates magnetic dipole of its own along axis of the spin. The magnitude of dipole is defined by nuclear magnetic moment. In the absence of an external magnetic field, all the spins have equivalent energy and are arranged randomly. When magnetic field is applied spins orient and can be aligned or opposed to the direction of an external magnetic field. The aligned configuration is stable and has lower energy, while the opposed has higher energy. The energy which will be absorbed by the atom is equal to the difference between the two spin states. The relaxation to the ground state is led by the emission of a radiofrequency photon, which is registered and gives the NMR signal of corresponding nuclei. The frequency is proportional to the applied magnetic field (Eq. 4) [18].

$$\nu = \frac{\gamma}{2\pi} B_0, \tag{4}$$

where ν – frequency, γ – magnetogyric ratio (constant for each type of nucleus), B_0 – applied magnetic field. During NMR measurements spin-relaxation time of the probes is recorded. Experimentally obtained relaxation time is proportional to the translational diffusion coefficient. From which the viscosity of the fluid can be recalculated.

Hypophosphite ($H_2PO_2^-$) ion was used as a viscosity probe in ^{31}P-NMR measurements. During them microviscosity of red cells was determined [19]. Using ^{19}F-NMR spectroscopy cytoplasmic microviscosity of *E. coli* cells was measured for nonspecific protein interactions characterisation. Results showed that viscosity of cytoplasm is around three times higher than in water. Globular proteins labelled with amino acid analogues (6F-tryptophan or 3F-tyrosine) were used for measurements [20].

EPR technique is based on similar concepts as NMR. However, in contrast to nuclear magnetic resonance, the spins are excited from electrons not from atom nuclei. In EPR spectroscopy, radiation

range is in gigahertz and unlike NMR, in electron paramagnetic resonance the frequency of radiation is kept constant while the magnetic field varies to obtain an absorption spectrum. When the magnetic field is applied the same energy split of spins happen; with the magnetic moment of the electron parallel with applied magnetic field having lower energy, while antiparallel has higher energy. With growing magnetic field strength, the energy difference between them increases linearly. The proportionality factor is the quantitative parameter for analysis. For example, free electron has the proportionality factor of 2.00232 [21]. It is necessary to mention that the unpaired electrons are also sensitive to their local environments. Nuclei can produce additional magnetic field. Interaction between the electron and the nuclei is called the hyperfine interaction. Additionally, hyperfine interaction can provide information about sample and its surroundings. The energy of an electron can be defined using Eq. 5. First term represents electron interaction with applied external magnetic field, second term describes hyperfine interaction [22]:

$$E = g\mu_B B_0 m_s + a m_s m_l, \tag{5}$$

where g – proportionality factor (g-factor), μ_B – Bohr magneton, B_0 – applied magnetic field, m_s – electron spin quantum number, m_l – nuclear spin quantum number, a – hyperfine coupling constant.

Using EPR method, microviscosity was successfully determined in model systems. 4-(methylamino)-2-ethyl-5,5-dimethyl-4-pyridine-2-yl-2,5-dihydro-1H-imidazol-1-oxyl (MEP) was used as the spin label and for experiments was dissolved in different water/glycerol mixtures. In low viscosity solutions, MEP EPR spectra was highly symmetric and showed narrow lines. In high viscosity solutions, EPR lines broadened, and signal amplitude was reduced. Spectral anisotropy increased with increasing surrounding viscosity. Furthermore, a rotational correlation time, which is dependent on microviscosity and molecular crowding, decreased in solutions with high glycerol content [23]. Another group of scientists were able to measure microviscosity of biological samples by using ^{13}C-labelled trityl spin probe (^{13}C-dFT). Experiments showed that ^{13}C-dFT EPR spectra peak broadening is consistent with increasing microviscosity. Water/glycerol solutions with increasing glycerol part were used to make a calibration curve. Peak linewidth depended linearly on viscosity. Using this EPR approach microviscosity of blood and interstitial fluids of living tissues were successfully assessed [24].

1.2.2 Fluorescent techniques

Microviscosity measurements with fluorescent probes are more advantageous than spectroscopic techniques because they provide rapid signal response and high spatial resolution. The most widespread fluorescent methods are fluorescence recovery after photobleaching (FRAP), fluorescence correlation spectroscopy (FCS), steady-state and time-resolved fluorescence anisotropy (FA), and fluorescent molecular rotors [12].

FRAP is a versatile tool for mobility of molecules characterisation in living cells. During FRAP analysis narrow confined area of fluorophores is illuminated and bleached by intensive laser pulse. As showed in Fig. 3A, surrounding molecules diffuse into bleached area and over time fluorescence intensity is regained. The recovery of the fluorescence is then analysed as a function of time (Fig. 3B). Rate of recovery depends on diffusion coefficient and binding of molecules within the analysed area. The analysis gives information about the rate of translation diffusion from which

microviscosity can be calculated. Green fluorescent protein (GFP) is usually used to tag non-fluorescent molecules [25].

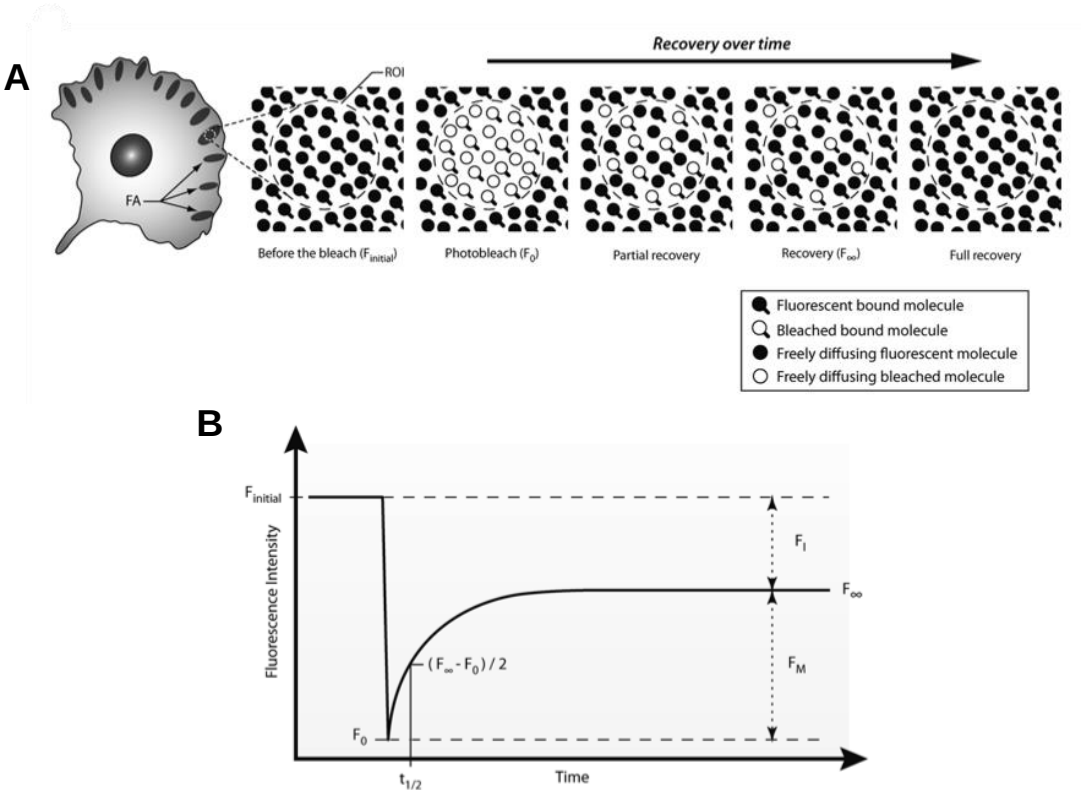

Fig. 3. *Principle of FRAP analysis. Bleaching and recovery of the fluorophores (A) and fluorescence intensity as a function of time (B)* [25].

During FRAP analysis, movement of the particle in a free-volume model with unrestricted diffusion is expressed by Stokes-Einstein formula [26]:

$$D = \frac{kT}{6\pi\eta R_h}, \tag{6}$$

where η – viscosity, D – diffusion coefficient, k – Boltzmann constant, T – absolute temperature, R_h – hydrodynamic radius of the particle. Movement of the particle by laterall diffusion in membrane is slower because of more viscous environment. Relationship of diffusion coefficient in two-dimensional movement and viscosity of membrane is described by the Saffman-Delbrück equation [26]:

$$D = \frac{kT}{4\pi\eta h}\left[\ln\left(\frac{2L_{SD}}{a}\right) - 0.5772\right], \tag{7}$$

where h – membrane bilayer thickness, L_{SD} – Saffman-Delbrück length, a – radius of transmembrane segment. FRAP can be used for numerous application purposes within the cell. For example, for protein movement characterisation inside mitochondria or nucleus, cell mitosis dynamics visualisation, or for observation of conformational changes of proteins [26,27].

Fluorescence correlation spectroscopy is another method for determination of diffusion coefficient. FCS measurements do not require high concentration of fluorophores and analyse only small volumes of fluid. FCS analyses temporal fluctuations of the fluorescence intensity over time. These fluctuations are caused by changes in the concentration of fluorescent particles within the volume of interest, i.e., detection volume. The analysis of FCS is based on Brownian motion of molecules. Obtained spectra of fluorescence fluctuations is fitted using autocorrelation function *G(τ)* (Eq. 8) [28].

$$G(\tau) = \frac{\langle I(t) \cdot I(t+\tau) \rangle}{\langle I(t) \rangle^2}, \tag{8}$$

where *I(t)* – fluorescence intensity as a function of time, τ – lag time. FCS principle is schematically shown in Fig. 4. Autocorrelation function has maximum value when $\tau = 0$. Over time it decreases because fluorophores diffuse from detection volume and average fluorescence intensity also decreases. The average time molecule spends in detection volume is equal to the time at which *G(τ)* decays to half of its maximum value [28].

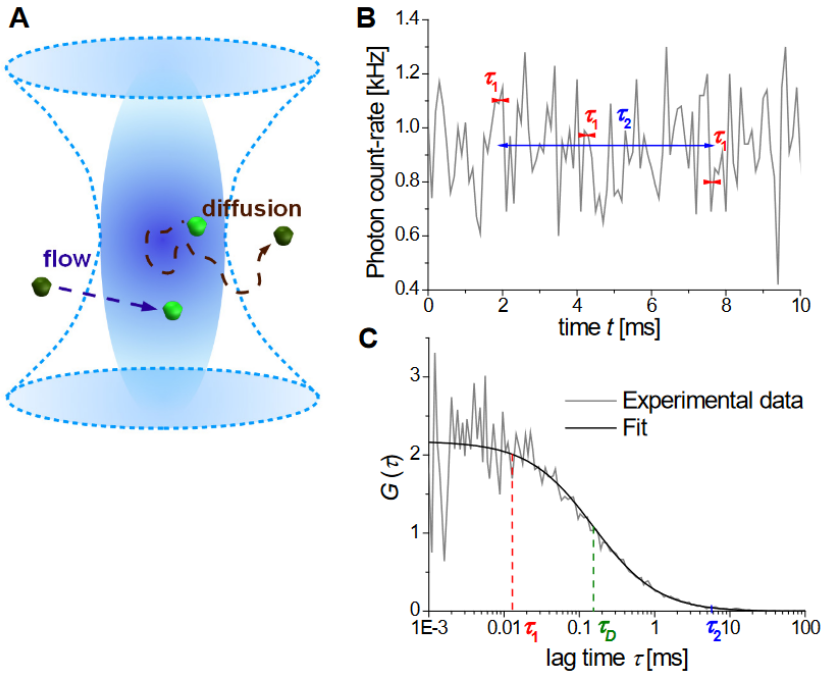

Fig. 4. *Schematic principle of fluorescence corelation spectroscopy (A). Examples of fluorescence fluctuations (B) and autocorrelation function fitting over time (C)* [28].

FCS can help to obtain information about the average number of fluorescent particles in the detection volume and their average diffusion time through the same volume [29]. Consequently, molecules concentration, kinetic rates or the viscosity of the media can be determined, too [30,31].

Fluorescence anisotropy is a measurement of rapidly changing orientation of the molecule. When fluorophore is excited, for example, with vertically polarised light, the emitted light will retain some of that polarisation based on how fast fluorophore rotates. If rotation is slow, the emission is highly polarised, and fluorescence has strong anisotropic properties. If rotation is fast, emitted light is highly depolarised and has low anisotropy (Fig. 5).

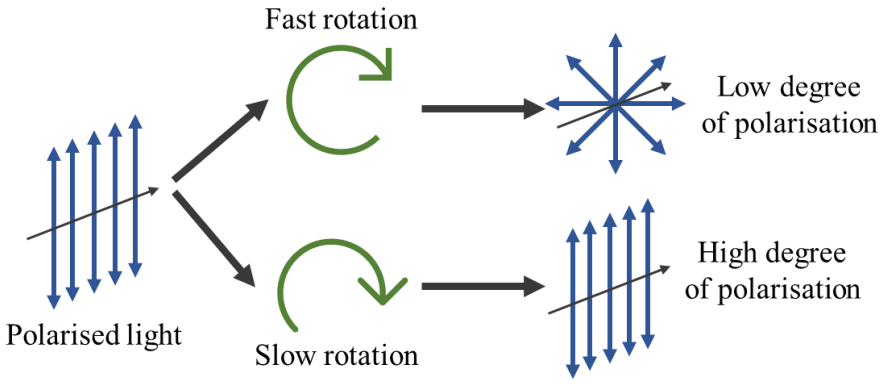

Fig. 5. *Scheme showing how rotation of fluorophores impact their fluorescence anisotropy.*

Polarised fluorescence emission has different horizontal and vertical components, and its anisotropy is expressed as follows [32,33]:

$$r = \frac{I_{\parallel} - I_{\perp}}{I_{\parallel} + 2I_{\perp}}, \tag{9}$$

where $I_{\parallel}$ – is the polarised component of fluorescence parallel to the polarised excitation beam, $I_{\perp}$ – is the polarised component of fluorescence perpendicular to the polarised excitation. The rotational correlation time of fluorescence anisotropy is analytical parameter which is directly related to the rotational diffusion of the fluorophore in the solution. Stokes-Einstein-Debye equation quantitatively relates correlation time (θ) and local viscosity (η) [32,33]:

$$\Theta = \frac{\eta V}{kT}, \tag{10}$$

where V – volume of rotating unit, k– Boltzmann constant, T – absolute temperature. Steady-state (r) and time-resolved ($r(t)$) anisotropy expressions are as follows [32,33]:

$$r = \frac{r_0}{1 + \frac{\tau}{\Theta}}, \tag{11}$$

$$r(t) = r_{\infty} + (r_0 - r_{\infty})e^{-\frac{t}{\theta}}, \tag{12}$$

where r_0 – maximum fluorescence anisotropy, r_{∞} – hindered anisotropy when $t = \infty$, τ – fluorescence lifetime.

T. Araiso and T. Koyama used steady-state anisotropy of 1,6-diphenyl-l,3,5-hexatriene (DPH) fluorophore to measure the membrane viscosity. Furthermore, they assessed how molecular length of fluorophore and quenchers in surrounding medium impact fluorescence anisotropy of DPH probe [34]. Recently, R. Kuriyama *et al.* developed two-dimensional viscosity mapping technique based on fluorescence anisotropy method. They successfully mapped viscosity of two miscible solutions in the microchannel (Fig. 6). Casein molecules labelled with fluorescein isothiocyanate were used as fluorescent probes [35].

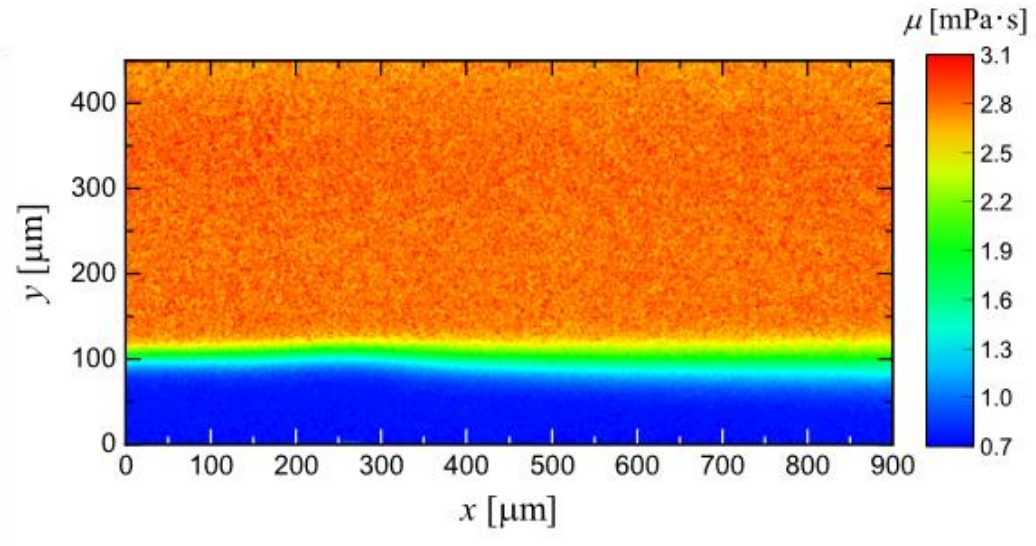

Fig. 6. *Map of viscosity in the microchannel obtained by steady-state anisotropy measurements* [35].

Zheng and his group analysed free and protein bound nicotinamide adenine dinucleotide (NADH) using time-resolved fluorescence anisotropy [36]. By comparing free and bound NADH rotational diffusion times they were able to separate two forms both *in vivo* and *in vitro*. This is important because healthy and cancerous cervical epithelial cells have different ratio of bound and free NADH. Furthermore, they were able to measure the microviscosity of NADH environment showing that fluorescence anisotropy technique is sensitive enough to record fluorescence of even relatively small molecules alike NADH [36].

1.2.3 Molecular rotors

Another fluorescent technique for measuring the viscosity is fluorescent molecular rotors. FMRs are the group of organic fluorophores, the spectroscopic properties of which is sensitive to the viscosity of a medium. Upon excitation, a fluorescent molecular rotor undergoes intramolecular rotation. Fluorescence intensity depends on the time molecule spends in the excited state before the rotation. Intramolecular rotation is fast in low viscosity solvents, which leads to fluorescence quenching and non-radiative relaxation. In contrast, in high viscosity solvents molecule is strongly immobilised and large-amplitude motions are hindered. Thus, rotation is slow and time the molecules spends in excited state is prolonged. This results in an increased fluorescence intensity. Besides the fluorescence intensity, fluorescence quantum efficiency and lifetime also increase.

To understand how microviscosity is related to the rates of intramolecular motion of molecular rotors few theories were developed. One of the first was Kramer's theory, which explored viscosity and temperature effect on isomeration of the molecule [37]. Förster and Hoffmann, who studied triphenylamine dyes and their fluorescence intensity dependence on viscosity, presented updated version of Kramer's theory [38]. They derived a relationship between fluorescence quantum yield (φ_f) and bulk viscosity (η) of the solvent at intermediate viscosity values:

$$\varphi_f = C\eta^x, \tag{13}$$

where C and x are constants. First synthesis and characterisation of molecular rotors marks the turn of the century [39]. These FMRs were based on malonitrile group, two of those – 9-(dicyanovinyl)-

julolidine (DCVJ) and 9-(2-carboxy-2-cyano)vinyl julolidine (CCVJ) – were used for viscosity sensing in phospholipid bilayers [40], polymers [41], and cell membranes [42]. Unfortunately, viscosity using these probes is assessed from the fluorescence intensity, which is concentration-dependent. To overcome this disadvantage three new types of fluorescent molecular rotors were introduced: ratiometric, lifetime-based and dual mode molecular rotors.

Ratiometric FMRs are fluorophores which have two fluorescence peaks; only one of which usually shows viscosity dependent intensity. These FMRs consist of two covalently bound fluorescent molecules. One molecule function as viscosity sensor, and another is used as reference for intensity measurements. One of the first ratiometric molecular rotors was reported by Haidekker and his colleagues [43]. They coupled 2-cyano-3-(4-dimethylaminophe-nyl)acrylic acid methyl ester (I) and 7-methoxycoumarin-3-carboxylic acid (II) (Fig. 7A). With increasing viscosity, only intensity of one peak (from molecule I) increased (Fig. 7B). After division of fluorescence emission peak value of the molecule I by peak value of the molecule II normalised intensity was acquired. This method eliminated the influence of dye concentration.

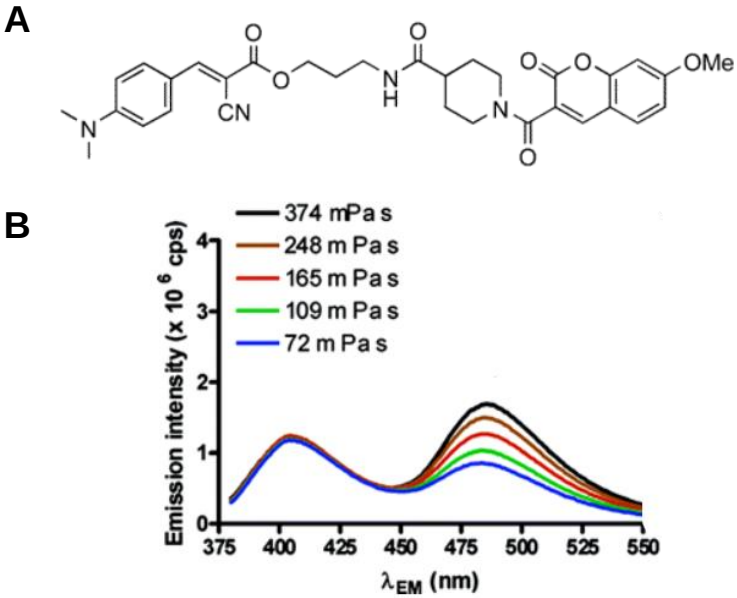

Fig. 7. *Molecular structure of Haidekker and his colleagues reported ratiometric FMR (A) and fluorescence spectra of FMR in ethylene glycol and glycerol mixtures (B)* [43].

Recently, Guanghan *et al.* investigated another ratiometric FMR [44]. They joined phenyl-substituted imidazole-fused rhodamine dye and graphene quantum dots (RV-1-GQDs) (Fig. 8A). Fluorescence emission spectra of this newly reported FMR also consists of two peaks. Unlike previously discussed fluorescent molecular rotor, both peaks showed viscosity dependence. Their intensity ratio increased with increasing viscosity (Fig. 8B). RV-1-GQDs was successfully applied for viscosity measurements in living systems in the range of 0–600 cP [44].

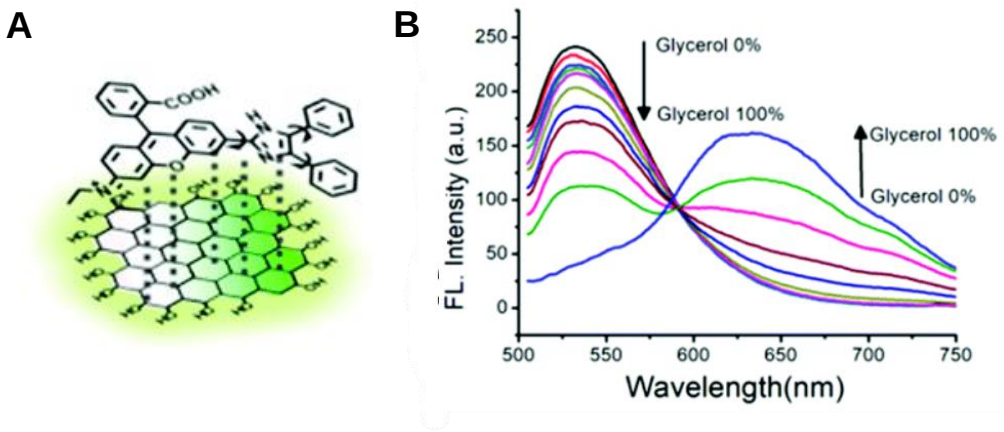

Fig. 8. *Molecular structure of Guanghan Li and his colleagues reported ratiometric FMR (A) and fluorescence spectra of FMR in PBS and glycerol mixtures (B)* [44].

Another type of fluorescent molecular rotors is lifetime-based FMRs. Lifetime is a great quantitative parameter for viscosity sensing because it is concentration independent parameter which gives reliable results in the absence of dye aggregation or fluorescence quenching. Combined with fluorescence lifetime imaging microscopy (FLIM) it enables measurements of large and heterogeneous cell area at the same time. Most of lifetime FMRs are based on BODIPY group. Dent *et al.* reported three new BODIPY-based fluorophores for viscosity sensing in model lipid bilayers [45]. This group tested molecular dynamics and found out preferred orientations and diffusion coefficients of FMRs in bilayers. Moreover, Dent and co-workers managed to determine viscosity of different type (liquid ordered (L_o) and liquid disordered (L_d)) giant unilamellar vesicles (GUVs) and thus separate these two phases (Fig. 9). All three FMRs favoured L_d phase more over L_o phase.

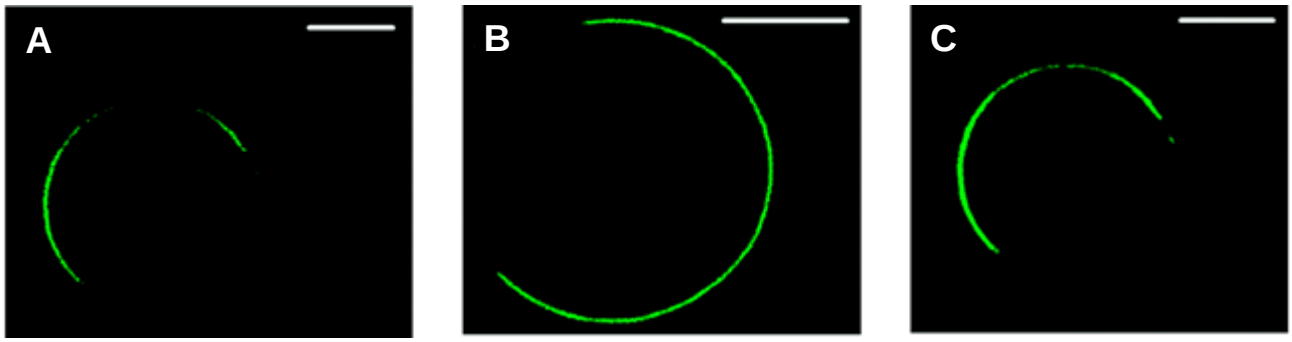

Fig. 9. *Confocal images of L_o–L_d phase separated DOPC/EYSM/Chol GUVs with investigated three different rotors (A–C). Scale bar is 10 μm* [45].

Measurements with dual mode molecular rotors employ both ratiometric and lifetime-based techniques for viscosity sensing. These FMRs eliminate dye concentration and optical properties impact of the solvent as well as other experimental or instrumental issues. Peng and colleagues reported the first dual mode molecular rotor [46]. Their pentamethine based dye RY3 with aldehyde substituent has two emission peaks (456 nm and 650 nm), where the red emission is enhanced by increasing viscosity. Furthermore, fluorescence lifetime of a dye was prolonged approximately seven times in viscous environment compared to non-viscous environment. RY3 dye can be used to image viscosity in cytoplasm of living cells, such as PC12 or MCF-7 breast cancer cells. Dual mode imaging provides full mapping of stained MCF-7 cells (Fig. 10) [46].

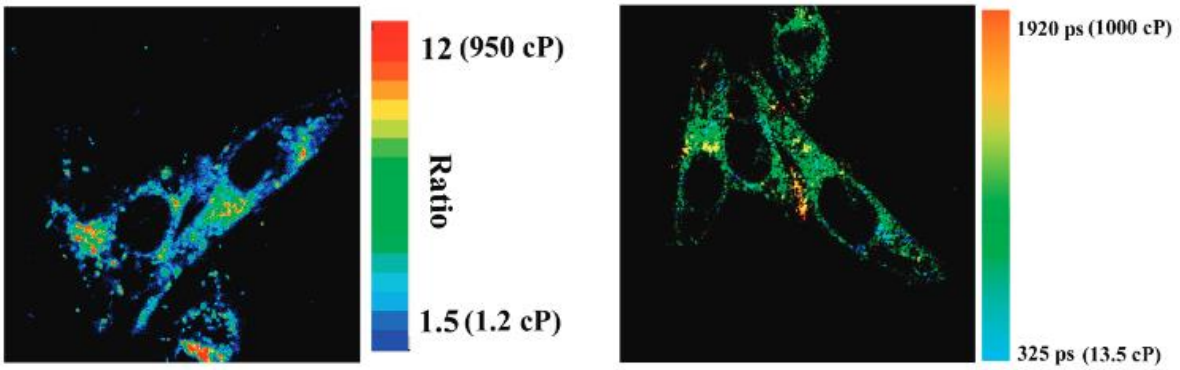

Fig. 10. *Ratiometry fluorescence (left) and FLIM (right) images of stained MCF-7 cells* [46].

Another dual mode fluorescent molecular rotor was presented by Vyšniauskas and his colleagues [47]. They explored conjugated porhyrin dimer and its ability to sense viscosity at microscopic level. This FMR can emit light in green (640 nm) and red (695 nm) region. Both emission peaks follow in the optical biological window which is a huge advantage and sets porphyrin-based FMR apart from other FMRs. Fluorescence intensity ratio (I_{640}/I_{695}) gives normalised intensity values. Intensity ratios increases thirty-two times in viscous fluid. Combination of both ratiometric and lifetime-based measurements give quantitative and dynamic information of a lipid-based environment (Fig. 11) [47].

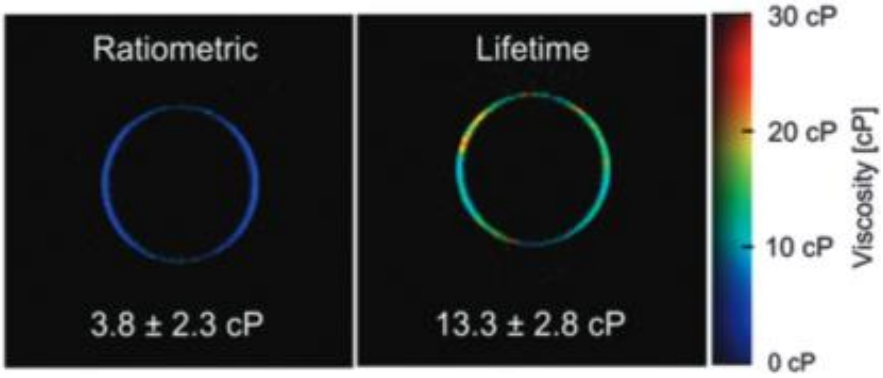

Fig. 11. *Ratiometric (left) and lifetime-based (right) viscosity maps of diphytanoylphosphatidylcholine monolayer in water/dodecane* [47].

In conclusion, fluorescent molecular rotors are excellent tool for measuring physical properties of the environment at molecular level. Measurements which involve FMRs are non-invasive, have great sensitivity and fast signal response. Furthermore, with FMRs viscosity imaging can be performed and powerful excitation laser is not needed as opposed to FRAP. In addition, equipment used in measurements is simple and there is only a small risk in sample damage.

1.3 BODIPY-based molecular rotors

4,4-difluoro-4-bora-3a,4a-diaza-*s*-indacene (BODIPY) was first discovered by two german scientists Treibs and Kreuzer in 1968 [48] and only after 1990 was recognised and studied intensively [49]. BODIPY dyes absorb ultraviolet light and their emission results in relatively sharp fluorescence peaks in a visible light spectrum. Absorption and emission wavelengths vary in between 470 nm and 530 nm. Furthermore, BODIPY dyes are photostable and have high fluorescence emission quantum

yield (>50 %) [50]. Most of these dyes are hydrophobic, but because of their zwitterionic form (Fig. 12), they can dissolve in a broad range of solvents [51].

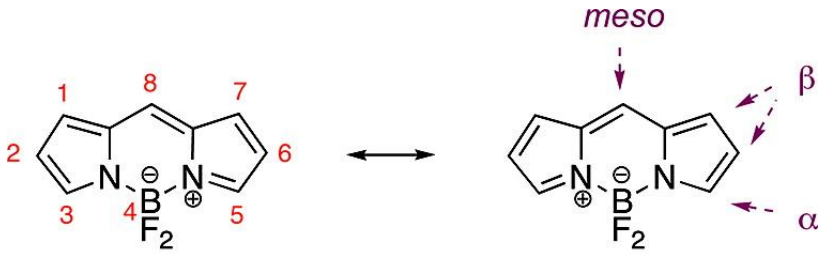

Fig. 12. *Molecular structure and zwitterionic form of BODIPY molecule* [51].

As mentioned previously, most of the BODIPY-based probes emit photons in a green spectral region. While working with biological samples, red or near-infrared light is more desirable to obtain deeper tissue penetration and minimise light scattering. Furthermore, red emitting FMRs can be used together with other fluorophores, e.g., GFP. To fulfil these requirements various structural modifications can be performed to tune spectroscopic properties of these dyes. New functional groups can be added to *α*-, *β*- or *meso*- positions to suppress core motion and/or extend π-conjugation [52]. Another approach is to add electron withdrawing (EWG) or electron donating (EDG) groups [53]. Unfortunately, these modifications usually result in decreased quantum yield [50].

Another type of modification is addition of particular substituents to direct FMRs to specific location of living cells. For instance, alkoxy groups (-$OC_{10}H_{21}$, -$OC_{16}H_{33}$ to name a few) are added to increase the lipophilicity of molecular rotors and enable easier penetration to hydrophobic cell membrane. Furthermore, the protein tag system (HaloTag) can be used to direct FMRs to endoplasmic reticulum, cellular cytoplasm or mitochondria [54,55].

Among all FMRs, BODIPY-C_{10} and BODIPY-C_{12} are the most popular molecular rotors (Fig. 13). They belong to the fluorescence lifetime-based type of molecular rotors. BODIPY-C_{10} and BODIPY-C_{12} have identical photophysical properties and differ only in the length of the hydrocarbon chain. BODIPY-C_{10}/C_{12} and other similar fluorophores have been used to measure microviscosity in aerosols [56], live cells [57], plasma membranes [58], model lipid membranes [45] and polymers [59]. Their main advantages are easy functionalisation, photostability, high extinction coefficient, and monoexponential decay [60]. The last one of which makes data analysis easier and enables their use in FLIM.

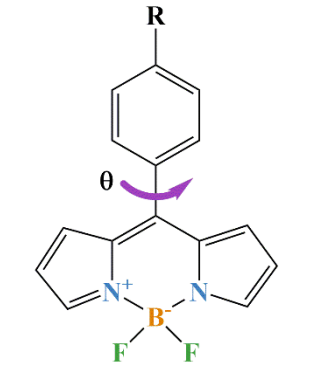

BODIPY-C_{10} R = -$OC_{10}H_{21}$
BODIPY-C_{12} R = -$OC_{12}H_{25}$

Fig. 13. *Molecular structure of BODIPY-C_{10}/C_{12} molecular rotors.*

BODIPY-based fluorophores with *meso*-phenyl ring are known two undergo conformational changes during intramolecular rotation [61]. The single carbon bond around which rotation occurs is indicated with violet arrow in Fig. 13. The quantitative connection between the energy barrier and the viscosity sensitivity of BODIPY molecular rotors was investigated using density functional theory calculations [7,62]. Simplified photophysical model for viscosity-sensitive BODIPY rotors and geometries of it at different stages are shown in Fig. 14.

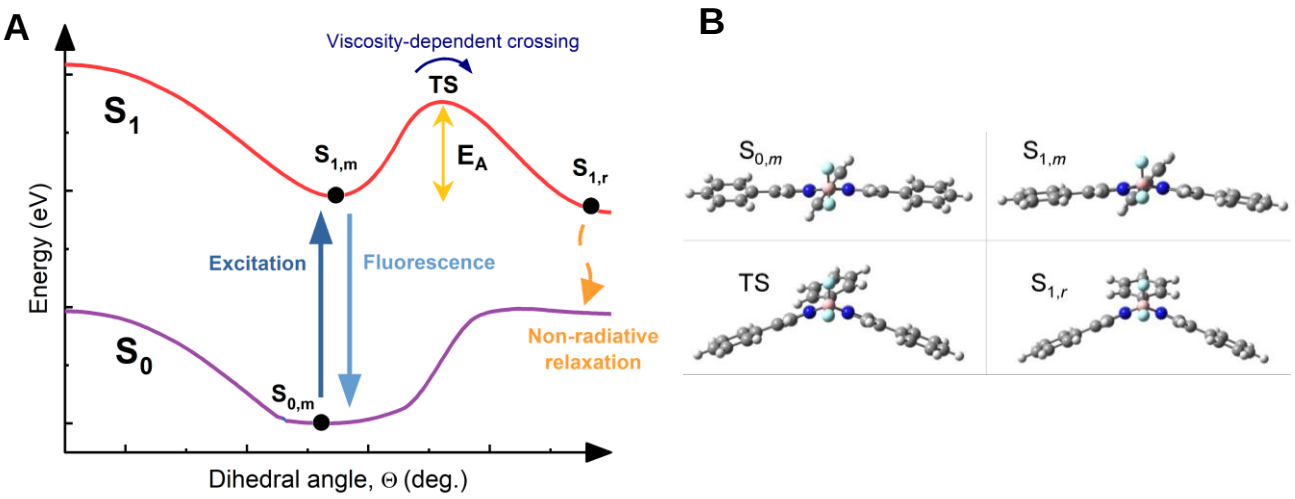

Fig. 14. *Simplified photophysical model for viscosity-sensitive BODIPY-based molecular rotors and geometries of it at different stages* [52].

First, molecule is excited from ground state ($S_{0,m}$) to fluorescent state at local minimum ($S_{1,m}$). Then, molecule can go through transition state (TS) and overcome relatively small energy barrier (E_A) to reach absolute minimum ($S_{1,r}$). Along this pathway geometry of molecule changes, as the rotor losses its planarity and becomes core-bended. In low-viscosity environment this energy barrier can be easily surpassed at room temperature. Remaining energy is released via non-radiative relaxation, which results in very weak fluorescence. While in high viscosity environment, molecular geometry changes are blocked and FMR relaxes to ground state by radiative decay. Hence, stronger fluorescence signal can be recorded. The crossing between $S_{1,m}$ and $S_{1,r}$ is largely viscosity-dependent and is the key factor which determines viscosity sensitivity.

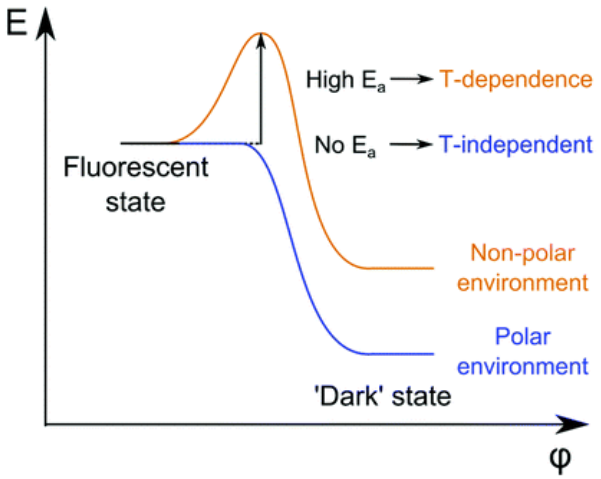

Fig. 15. *Simplified photophysical model for temperature and polarity sensitivity of BODIPY-based molecular rotors* [60].

The same energy barrier for non-radiative decay is responsible for sensitivity to temperature and polarity (Fig. 15) [60]. If FMR is sensitive to temperature energy barrier is high (>120 meV) [53]. With increasing temperature molecule has more thermal energy to cross it. Thus, with increasing temperature fluorescence intensity weakens and decay time shortens. Similar trends are also seen in polarity sensitivity. In non-polar environment FMR favours radiative decay pathway. In contrary, in polar environment it relaxes to ground sate non-radiatively. Therefore, when moving from hydrophobic to hydrophilic conditions fluorescence intensity and lifetime decreases.

2. METHODS AND MATERIALS

2.1 Dyes, reagents, and solvents

Stock solutions of all fluorophores were prepared in toluene (2 mM) and diluted for further experiments in solvents or their mixtures of interest. Cyclohexane, chloroform, dichloromethane (DCM), dimethyl sulfoxide (DMSO), toluene, methanol, castor oil, and glycerol were obtained from Sigma-Aldrich at spectroscopic grade if not stated otherwise and used without any further purification. The viscosities of toluene/castor oil and methanol/glycerol mixtures were measured by using a vibrational viscometer (SV10, A&D) at room temperature.

2.2 Absorption, steady-state, and time-resolved fluorescence

Absorption spectra were recorded using a Jasco V-670 spectrophotometer. Fluorescence spectra measurements were done with Edinburgh-F900 (Edinburgh Instruments) fluorimeter. The WhiteLase Micro (Fianium) laser with bandpass filters (ThorLabs) with 10 nm bandwith centred at 520 nm (BP-Ph-oMethyl), 540 nm (BP-Ph-oMethyl-NO_2, BP-Vinyl-C_{16}) or 570 nm (BP-Vinyl,BP-Vinyl-NO_2, BP-C-C-Ph, BP-C-C-Ph-C_{16}, BP-Ph, BP-Ph-mMethyl, BP-Ph-mMethyl-C_{16}, BP-Ph-mMethyl-NO_2) was used as an excitation source. Fluorescence decays were measured with aforementioned Edinburgh-F900 fluorimeter using the same excitation source. Decays were recorded with 5000 counts at the peak of the decay with 20 ns with 4096 channels. Measuring method was time-correlated single photon counting (TCSPC). For temperature measurements, dye solutions were heated using an Alpha RA 8 thermostat (LAUDA). For all spectroscopic measurements quartz cuvettes (10 mm) were used. The concentration of dyes varied from 2 to 10 μM.

2.3 Dependency on solvent polarity, viscosity, and temperature

Dependency on solvent polarity was investigated by measuring absorption, fluorescence spectra and time-resolved fluorescence decay in different polarity solvents. Cyclohexane was chosen as least polar solvent and methanol as most polar one. Orientation polarisation (*Δf*) was chosen as quantitative parameter to characterise polarity of solvents. It was calculated using Lippert's equation [63] (Eq. 14).

$$\Delta f = \frac{\varepsilon - 1}{2\varepsilon + 1} - \frac{n^2 - 1}{2n^2 + 1}, \tag{14}$$

where ε – dielectric constant, n – refractive index. Sensitivity to viscosity of surrounding environment were done in polar methanol, glycerol and non-polar toluene, castor oil solvents or in their mixtures. This covered viscosity range from 0.6 to 920 cP. Temperature sensitivity measurements were performed by heating dye solutions from 10 ˚C (283 K) to 70 ˚C (343 K). For molecules which did not show strong dependency on viscosity, activation energy (E_a) for non-radiative decay pathway was obtained by fitting temperature-dependent lifetimes in toluene with Eq. 15.

$$\tau = \frac{1}{k_x + k_{nr,max} e^{-\frac{E_a}{kT}}}, \tag{15}$$

where τ – fluorescence lifetime, k_x – the sum of radiative and all temperature-independent non-radiative decay rates leading to the relaxation from the excited state, $k_{nr,max}$ – maximum temperature-dependent decay rate, k – Boltzmann constant, T – absolute temperature. While for viscosity-sensitive molecules, viscosity of a medium was also considered when calculating activation energy (Eq. 16). The following equation is extended version of Förster-Hoffmann equation and characterises viscosity sensitivity over a relatively large viscosity range.

$$\tau = \frac{1}{\frac{1}{a_1\eta^{a_2} + a_3} e^{\frac{a_4}{T}} + a_5}, \tag{16}$$

where η – viscosity, a_1–a_5 – fitting parameters. When molecule is almost temperature-insensitive, then Eq. 16 can be simplified using $e^{\frac{a_4}{T}} = c$,

$$\tau = \frac{1}{\frac{c}{a_1\eta^{a_2} + a_3} + a_5} = \frac{1}{\frac{1}{\frac{a_1}{c}\eta^{a_2} + \frac{a_3}{c}} + a_5} = \frac{1}{\frac{1}{a_1'\eta^{a_2} + a_3'} + a_5}. \tag{17}$$

Relative sensitivity to viscosity was quantified using Förster-Hoffmann equation (Eq. 18). Higher the value x, stronger the sensitivity.

$$\tau = C\eta^x, \tag{18}$$

where τ – fluorescence lifetime, C and x – constants, η – viscosity.

2.4 Data analysis

Fluorescence decays were fitted using Edinburgh-F900 software package. Intensity-weighted lifetimes were calculated using Eq. 19:

$$\tilde{\tau} = \frac{\sum_i a_i\tau_i^2}{\sum_i a_i\tau_i}, \tag{19}$$

where a is an amplitude value and τ is the lifetime value. The goodness-of-fit parameter (χ^2) values was 1.5 or less. Further data processing and analysis was performed using OriginPro 2018 (OriginLab).

3. RESULTS AND DISCUSSION

The main focus of the research presented in this work was to characterise new BODIPY-based molecular rotors and to assess how changes in the molecular structure, e.g., prolonged conjugated system and/or substituents, influence their spectroscopic properties and sensitivity to the physical properties of a medium. Absorption and fluorescence emission spectra as well as time-resolved fluorescence decays have been recorded to characterise spectroscopic properties of the samples. Dependencies on solvent polarity, viscosity, and temperature were measured. All investigated fluorophores were divided into three groups based on their molecular structure and will be discussed in following chapters separately.

3.1 BP-Vinyl fluorophores

The first group of molecules contain BP-Vinyl fluorophores (Fig. 16). They have two vinyl (H-C=CH_2) functional groups attached to 2- and 6- position of the BODIPY core and *meso*-phenyl substituent which is unsubstituted for BP-Vinyl or has either alkoxy (-$OC_{16}H_{33}$) or nitro (-NO_2) substituent on *para* position of the ring respectively for BP-Vinyl-C_{16} and BP-Vinyl-NO_2. Vinyl groups were attached to the BODIPY core in order to extend π-conjugation and red-shift absorption and fluorescence spectra.

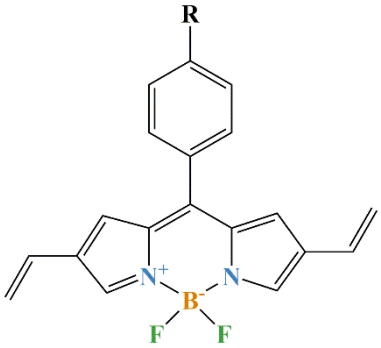

BP-Vinyl R = -H
BP-Vinyl-C_{16} R = -$OC_{16}H_{33}$
BP-Vinyl-NO_2 R = -NO_2

Fig. 16. *The molecular structures of BODIPY derivatives (BP-Vinyl, BP-Vinyl-C_{16}, BP-Vinyl-NO_2).*

3.1.1 Absorption and fluorescence spectra

The absorption spectra of BP-Vinyl molecules consist of the main absorption band at 560–600 nm and a higher energy band located at 350–450 nm (Fig. 17A). Addition of electron-withdrawing nitro group shifted absorption maximum by 17 nm towards red part of the visible spectrum. While addition of electron donating alkoxy group with sixteen carbon atoms resulted in 23 nm shift towards blue part and a little bit more broadened absorption peak compared to unsubstituted BP-Vinyl fluorophore. Similar trends are seen in the fluorescence spectra as well (Fig. 17B). BP-Vinyl fluorescence emission maximum is located at 620 nm with Stokes shift of 1083 cm^{-1}. BP-Vinyl-C_{16} and BP-Vinyl-NO_2 maximum and Stokes shift values are 614 nm (1635 cm^{-1}) and 650 nm (1338cm^{-1}), respectively.

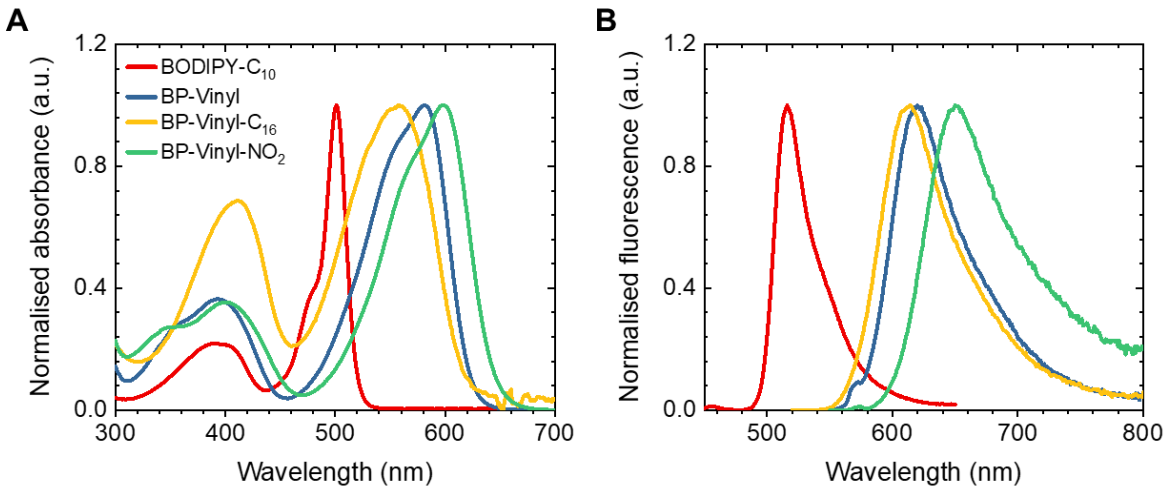

Fig. 17. *Absorption (A) and fluorescence (B) spectra of BP-Vinyl (blue), BP-Vinyl-C_{16} (yellow), BP-Vinyl-NO_2 (green) molecules compared to BODIPY-C_{10} (red) molecular rotor in toluene.*

Compared to widely used BODIPY-C_{10} fluorophore the main absorption and fluorescence peaks are red-shifted due to an increased electron conjugation. Experimental values of absorption (λ_{Abs}) and fluorescence (λ_{Fl}) maximum as well as Stokes shifts (ν_S) and molar extinction coefficients (ε_e) of BODIPY-C_{10}, BP-Vinyl, BP-Vinyl-C_{16} and BP-Vinyl-NO_2 molecules in toluene are presented in Table 1.

Table 1. *Experimental values of absorption (λ_{Abs}) and fluorescence (λ_{Fl}) maximum, Stokes shifts (ν_S) and molar extinction coefficients (ε_e) of BODIPY-C_{10}, BP-Vinyl, BP-Vinyl-C_{16} and BP-Vinyl-NO_2 molecules in toluene.*

Molecule	**λ_{Abs}, nm**	**λ_{Fl}, nm**	**ν_S, cm^{-1}**	**ε_e, M^{-1}·cm^{-1}**
BODIPY-C_{10}	501	516	580	$6.4\cdot10^4$
BP-Vinyl	581	620	1083	$1.4\cdot10^4$
BP-Vinyl-C_{16}	558	614	1635	$1.5\cdot10^4$
BP-Vinyl-NO_2	598	650	1338	$1.2\cdot10^4$

3.1.2 Dependency on solvent viscosity

Firstly, the sensitivity to viscosity of the new derivatives was explored. The majority of observed fluorescence decays were monoexponential. The average lifetimes of biexponential decays were calculated using Eq. 19. Biexponential decays were obtained in castor oil owing to its small contribution of autofluorescence. Viscosity sensitivity of fluorophores are depicted in Fig. 18. Almost no sensitivity to viscosity were seen for BP-Vinyl and BP-Vinyl-C_{16} dyes as their lifetimes increased only by 24 % (from 1.88 to 2.33 ns) and 44 % (from 2.40 to 3.45 ns). Both molecules also showed low x values (0.03 and 0.06 respectively) from Förster-Hoffmann fits. BP-Vinyl-NO_2 showed approximately three times longer fluorescence decay time in viscous non-polar castor oil solvent in contrast to non-viscous non-polar toluene solvent. x value also increased almost six times compared to BP-Vinyl which coincides with increased viscosity sensitivity. BP-Vinyl-NO_2 sensitivity is similar to BODIPY-C_{10} molecule while lifetime values are much shorter. Among all three BP-Vinyl molecules only the BP-Vinyl-NO_2 molecule could be used as viscosity sensor.

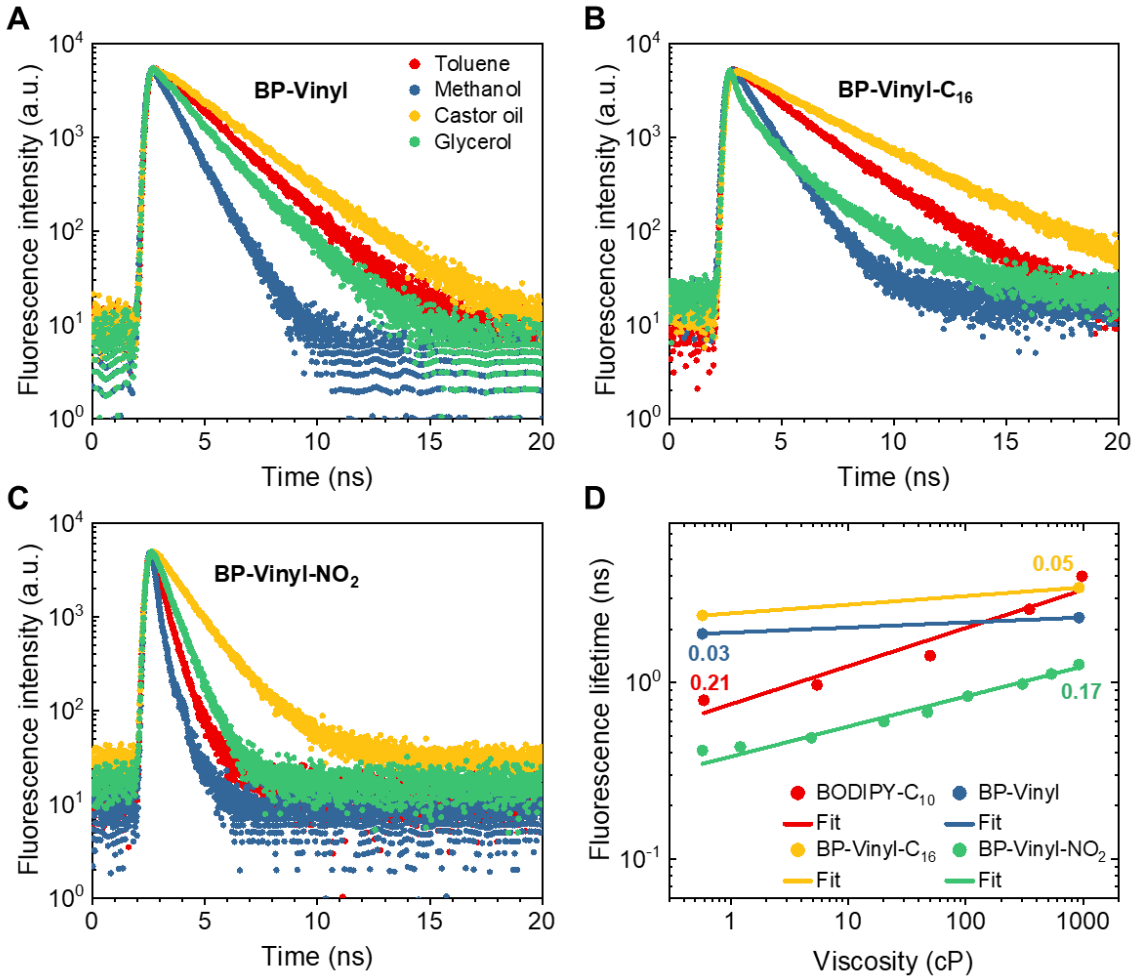

Fig. 18. *Time-resolved fluorescence decays in different viscosity solvents of BP-Vinyl (A), BP-Vinyl-C_{16} (B), BP-Vinyl-NO_2 (C) and fluorescence lifetimes (D) of BODIPY-C_{10} (red), BP-Vinyl (blue), BP-Vinyl-C_{16} (yellow), BP-Vinyl-NO_2 (green) obtained in different solvents with respect to the viscosity of these solvents. x values from fitting with Eq. 18 that show the extent of viscosity sensitivity are also shown.*

New viscosity probe (BP-Vinyl-NO_2) and its viscosity sensitivity was further analysed in more viscous environment (>1000 cP) in cold glycerol. Glycerol is a viscous solvent which is known to have glass transition temperature at 190 K, by cooling it down viscosity range can be extended from $1.7 \cdot 10^3$ cP to $1.6 \cdot 10^{11}$ cP. Time-resolved fluorescence decays in cold glycerol are shown in Fig. 19A. Viscosity-dependent lifetimes (Fig. 19B) were fitted using Eq. 17. Obtained fitting parameters are shown in Table 2.

Table 2. *Obtained fitting parameters from the fit in Fig. 19B used with Eq. 17.*

Molecule	$\mathbf{a_1'}$	$\mathbf{a_2}$	$\mathbf{a_3'}$	$\mathbf{a_5}$
BP-Vinyl-NO_2	50.77	0.39	82.48	$3.44 \cdot 10^{-4}$

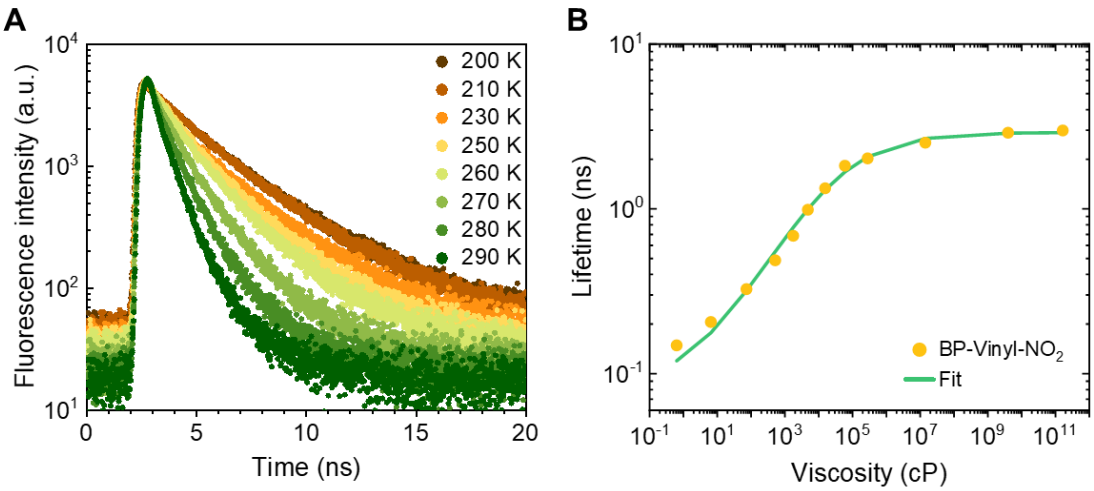

Fig. 19. *Time-resolved fluorescence decays in glycerol at different temperatures (A) and fluorescence lifetimes (B) obtained in cooled glycerol and room temperature methanol-glycerol mixtures with respect to the viscosity of these solvents of BP-Vinyl-NO_2 viscosity probe.*

BP-Vinyl-NO_2 viscosity probe can be used to sense viscosity up to 10^6 cP. While commonly used viscosity sensor BODIPY-C_{12} can only probe viscosity in the range of 5–1500 cP [57].

3.1.3 Dependency on solvent polarity

Secondly, the sensitivity to polarity was assessed. Absorption and fluorescence spectra of the BP-Vinyl fluorophores were not affected by solvotochromism. Absorption and fluorescence maximum were in the same spectral region (520– 680 nm), peak value varied around 15–25 nm (from non-polar cyclohexane to very polar DMSO).

Lifetime values of all three fluorophores decreased with increasing polarity (Fig. 20). BP-Vinyl-NO_2 stood out among all three dyes; the addition of EWG suppressed its sensitivity to polarity four times compared to BP-Vinyl. Additionally, compared to the most widely used BODIPY molecular rotor BODIPY-C_{10}, BP-Vinyl-NO_2 showed even less sensitivity to the polarity of solvent. Both BP-Vinyl and BP-Vinyl-C_{16} molecules exhibited similar sensitivity to polarity, with alkoxy-substituted one showing a little bit stronger dependency. Gradually decreasing lifetime value with increasing solvent polarity is desired property for a polarity sensor. BP-Vinyl-C_{16} satisfies this requirement and therefore could be used as polarity sensor.

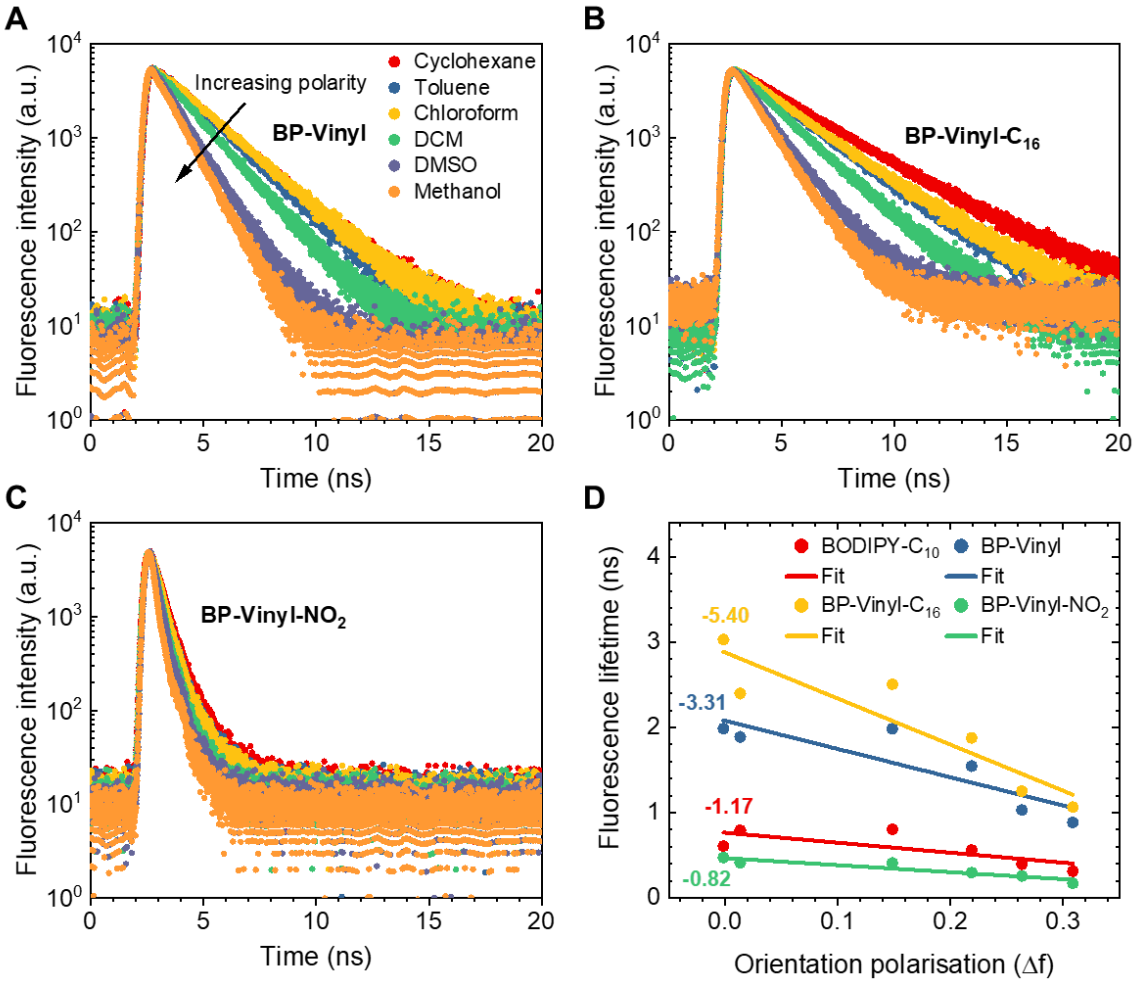

Fig. 20. *Time-resolved fluorescence decays in different polarity solvents of BP-Vinyl (A), BP-Vinyl-C_{16} (B), BP-Vinyl-NO_2 (C) and fluorescence lifetimes (D) of BODIPY-C_{10} (red), BP-Vinyl (blue), BP-Vinyl-C_{16} (yellow), BP-Vinyl-NO_2 (green) obtained in different solvents with respect to the orientation polarisation of these solvents. Slope values of linear fits are also shown.*

3.1.4 Dependency on solvent temperature

Lastly, the temperature dependency experiments were performed. The temperature measurements are important not only for determining sensitivity of fluorophore to it but also for finding activation energy barrier value for non-radiative decay pathway. Temperature sensitivity was evaluated in toluene, a low-viscosity solvent. BP-Vinyl and BP-Vinyl-C_{16} showed modest sensitivity to increasing temperature (Fig. 21A, B). Moreover, it showed similar sensitivity to the temperature as BODIPY-C_{10} fluorophore. In contrast, addition of nitro group supressed temperature sensitivity (Fig. 21C). BP-Vinyl and BP-Vinyl-C_{16} showed longer lifetime values, while BP-Vinyl-NO_2 showed shorter ones as expected in a low-viscosity solvent.

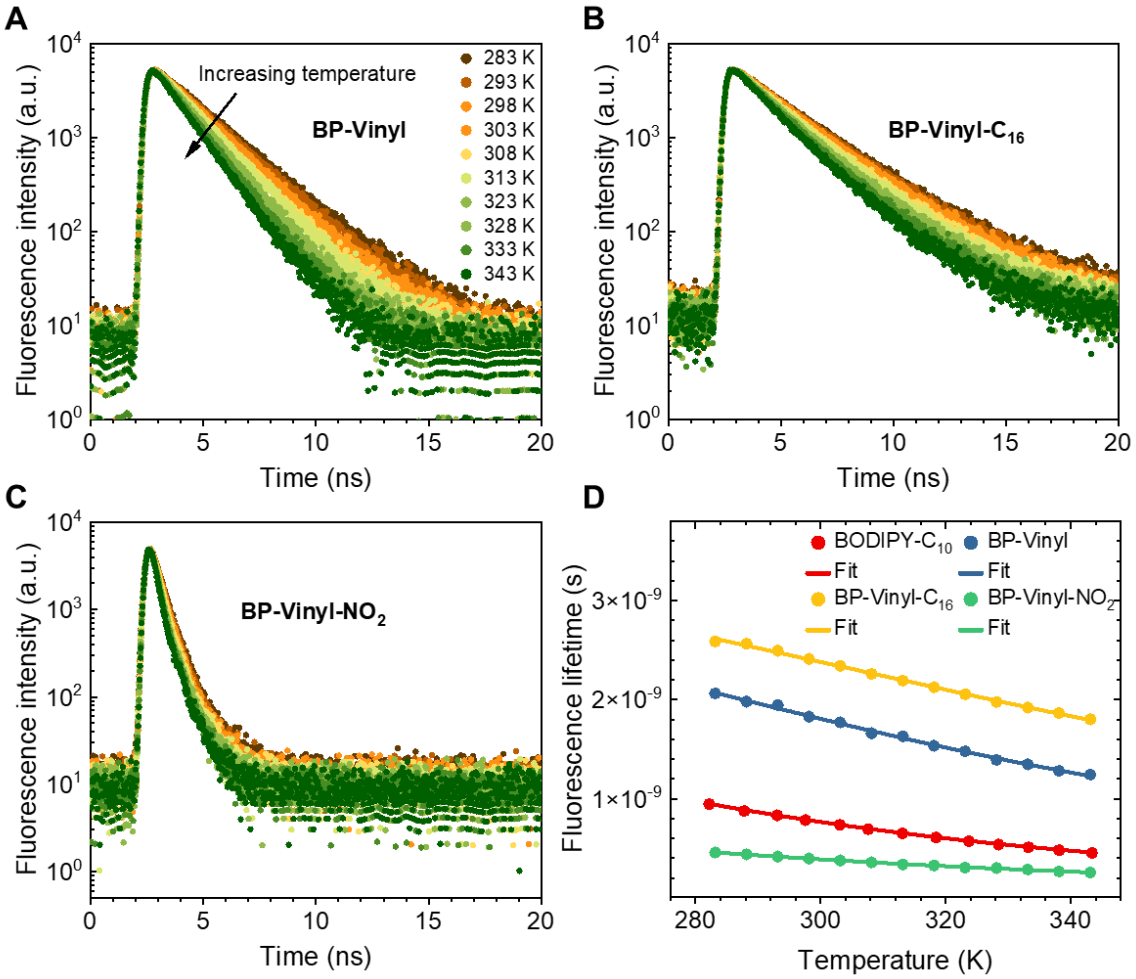

Fig. 21. *Time-resolved fluorescence decays of BP-Vinyl (A), BP-Vinyl-C_{16} (B), BP-Vinyl-NO_2 (C) and fluorescence lifetimes (D) of BODIPY-C_{10} (black), BP-Vinyl (red), BP-Vinyl-C_{16} (blue), BP-Vinyl-NO_2 (green) obtained in toluene at different temperatures.*

Experimental values of the sum of radiative and all temperature-independent non-radiative decay rates (k_x), maximum temperature-dependent decay rate ($k_{nr,max}$) and activation energy (E_a) of BODIPY-C_{10}, BP-Vinyl, BP-Vinyl-C_{16} and BP-Vinyl-NO_2 molecules in toluene are shown in Table 3. Values were obtained after fitting temperature-dependent lifetimes with Eq. 15.

Table 3. *Experimental values of the sum of radiative and all temperature-independent non-radiative decay rates (k_x), maximum temperature-dependent decay rate ($k_{nr,max}$) and activation energy (E_a) of BODIPY-C_{10}, BP-Vinyl, BP-Vinyl-C_{16}, BP-Vinyl-NO_2 molecules in toluene.*

Molecule	**k_x, ns^{-1}**	**$k_{nr,max}$, ns^{-1}**	**E_a, meV**
BODIPY-C_{10}	0.50±0.03	290±47	152±5
BP-Vinyl	0.31±0.03	83±50	151±19
BP-Vinyl-C_{16}	0.29±0.02	43±20	149±16
BP-Vinyl-NO_2	0.99±0.21	193±87	124±15

Addition of EDG lowered energy barrier value only by 2 meV and reduced non-radiative decay rate twice compared to BP-Vinyl molecule. While addition of a nitro group lowered energy barrier by 27 meV and increased non-radiative decay rate more than twice, which led to improved viscosity sensitivity similarly as in the previous work of Maleckaitė *et al.* [52].

3.2 BP-C-C-Ph fluorophores

The second group of molecules consists of two BP-C-C-Ph fluorophores (Fig. 22). They have prolonged conjugated system through attachment of two phenyl moieties at 2- and 6- position of BODIPY core molecule via triple carbon-carbon bond. Along with *meso*-phenyl substituent which is unsubstituted for BP-C-C-Ph or has alkoxy (-$OC_{16}H_{33}$) substituent on para position of the ring for BP-C-C-Ph-C_{16} as similarly observed in BP-Vinyl fluorophores.

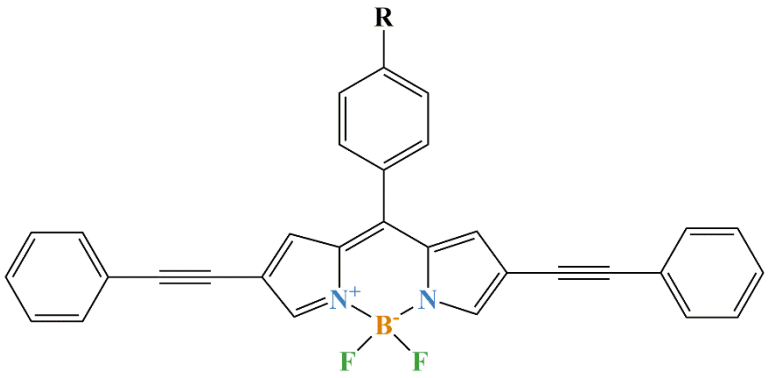

BP-C-C-Ph R = -H
BP-C-C-Ph-C_{16} R = -$OC_{16}H_{33}$

Fig. 22. *The molecular structures of BODIPY derivatives (BP-C-C-Ph and BP-C-C-Ph-C_{16}).*

3.2.1 Absorption and fluorescence spectra

The absorption spectra of BP-C-C-Ph molecules consist of two absorption bands. The main absorption band is located at 580–600 nm, and higher energy band is at 350–450 nm (Fig. 23A). Absorption spectra is similar to BP-Vinyl molecules. Addition of alkoxy group shifted peak position only by 7 nm towards blue part of a spectrum. The same trends are seen in the fluorescence spectra as well (Fig. 23B). BP-C-C-Ph and BP-C-C-Ph-C_{16} maximum and Stokes shift values are 638 nm (1048 cm^{-1}) and 628 nm (997 cm^{-1}), respectively. Compared to widely used BODIPY-C_{10} fluorophore and BP-Vinyl dyes the main absorption and fluorescence peaks are red-shifted due to prolonged electron conjugation.

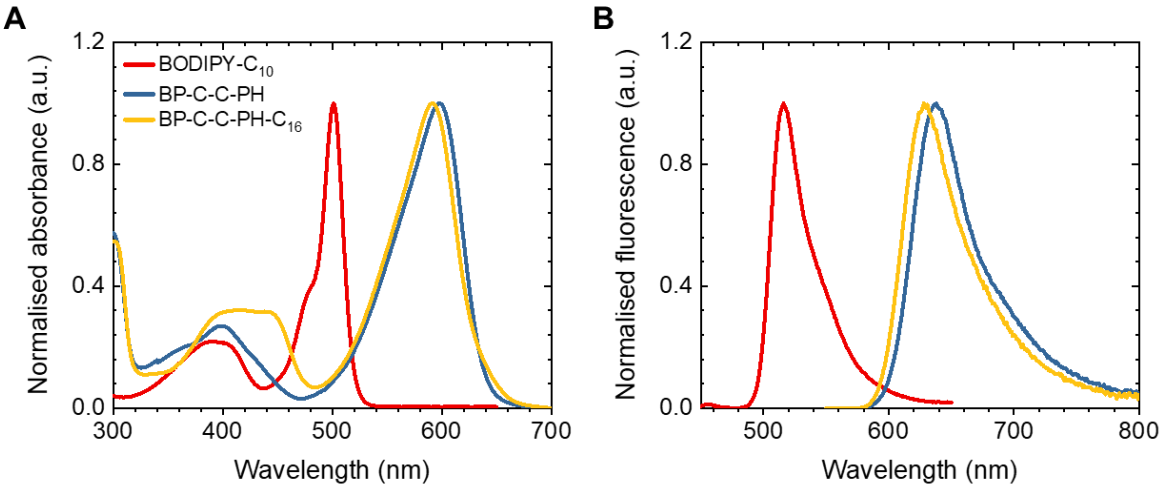

Fig. 23. *Absorption and fluorescence spectra of BP-C-C-Ph (blue), BP-C-C-Ph-C_{16} (yellow) molecules compared to BODIPY-C_{10} (red) molecular rotor in toluene.*

Experimental values of absorption (λ_{Abs}) and fluorescence (λ_{Fl}) maximum, Stokes shifts (ν_S) and molar extinction coefficients (ε_e) of BODIPY-C_{10}, BP-C-C-Ph and BP-C-C-Ph-C_{16} molecules in toluene are presented in Table 4.

Table 4. *Experimental values of absorption (λ_{Abs}) and fluorescence (λ_{Fl}) maximum, Stokes shifts (ν_S) and molar extinction coefficients (ε_e) of BODIPY-C_{10}, BP-C-C-Ph and BP-C-C-Ph-C_{16} molecules in toluene.*

Molecule	λ_{Abs}, nm	λ_{Fl}, nm	ν_S, cm^{-1}	ε_e, $M^{-1}\cdot cm^{-1}$
BODIPY-C_{10}	501	516	580	$6.4\cdot10^4$
BP-C-C-Ph	598	638	1048	$4.3\cdot10^4$
BP-C-C-Ph-C_{16}	591	628	997	$5.6\cdot10^4$

3.2.2 Dependency on solvent viscosity

First of all, dependency on solvent viscosity was evaluated. Viscosity sensitivity of fluorophores are depicted in Fig. 24. All fluorescent decays were monoexponential except for the dye solutions in castor oil. The average lifetimes of biexponential decays were calculated using Eq. 19. BP-C-C-Ph-C_{16} molecule was insoluble in glycerol, therefore no corresponding fluorescence decay is shown (Fig. 24B).

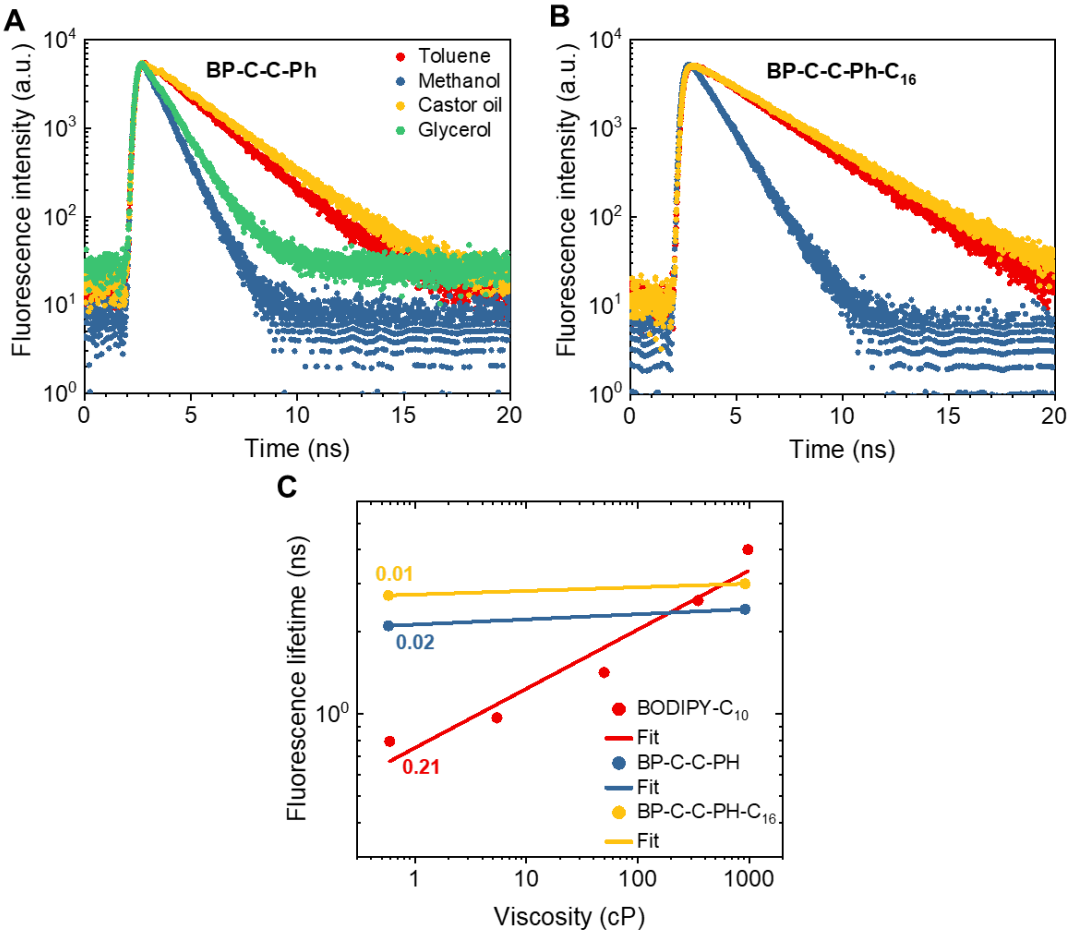

Fig. 24. *Time-resolved fluorescence decays in different viscosity solvents of BP-C-C-Ph (A), BP-C-C-Ph-C_{16} (B) and fluorescence lifetimes (C) of BODIPY-C_{10} (red), BP-C-C-Ph (blue), BP-C-C-Ph-C_{16} (yellow) obtained in different solvents with respect to the viscosity of these solvents. x values from fitting with Eq. 18 that show the extent of viscosity sensitivity are also shown.*

Both BP-C-C-Ph and BP-C-C-Ph-C_{16} fluorophores are viscosity insensitive. Their lifetimes increased only by 15 % (from 2.10 to 2.42 ns) and 10 % (from 2.72 to 3.00 ns), respectively. *x* values from Förster-Hoffmann fits were only 0.02 for BP-C-C-Ph and 0.01 for BP-C-C-Ph-C_{16} molecule. Neither of both molecules could be applied as viscosity sensors.

3.2.3 Dependency on solvent polarity

Furthermore, the polarity sensitivity of BP-C-C-Ph and BP-C-C-Ph-C_{16} molecules was examined. None of the BP-C-C-Ph fluorophores absorption and fluorescence spectra was affected by solvotochromism. Absorption maximum value varied in between 590 nm and 610 nm, while fluorescence maximum varied from 640 to 660 nm from cyclohexane to DMSO solvents.

Lifetime values of both fluorophores decreased gradually with increasing polarity (Fig. 25). Both BP-C-C-Ph and BP-C-C-Ph-C_{16} molecules showed similar sensitivity to polarity, with alkoxy-substituted one showing a little bit stronger dependency and longer lifetime values. As well as BP-Vinyl-C_{16}, both BP-C-C-Ph and BP-C-C-Ph-C_{16} fluorophores could be applied to probe polarity of the surrounding environment.

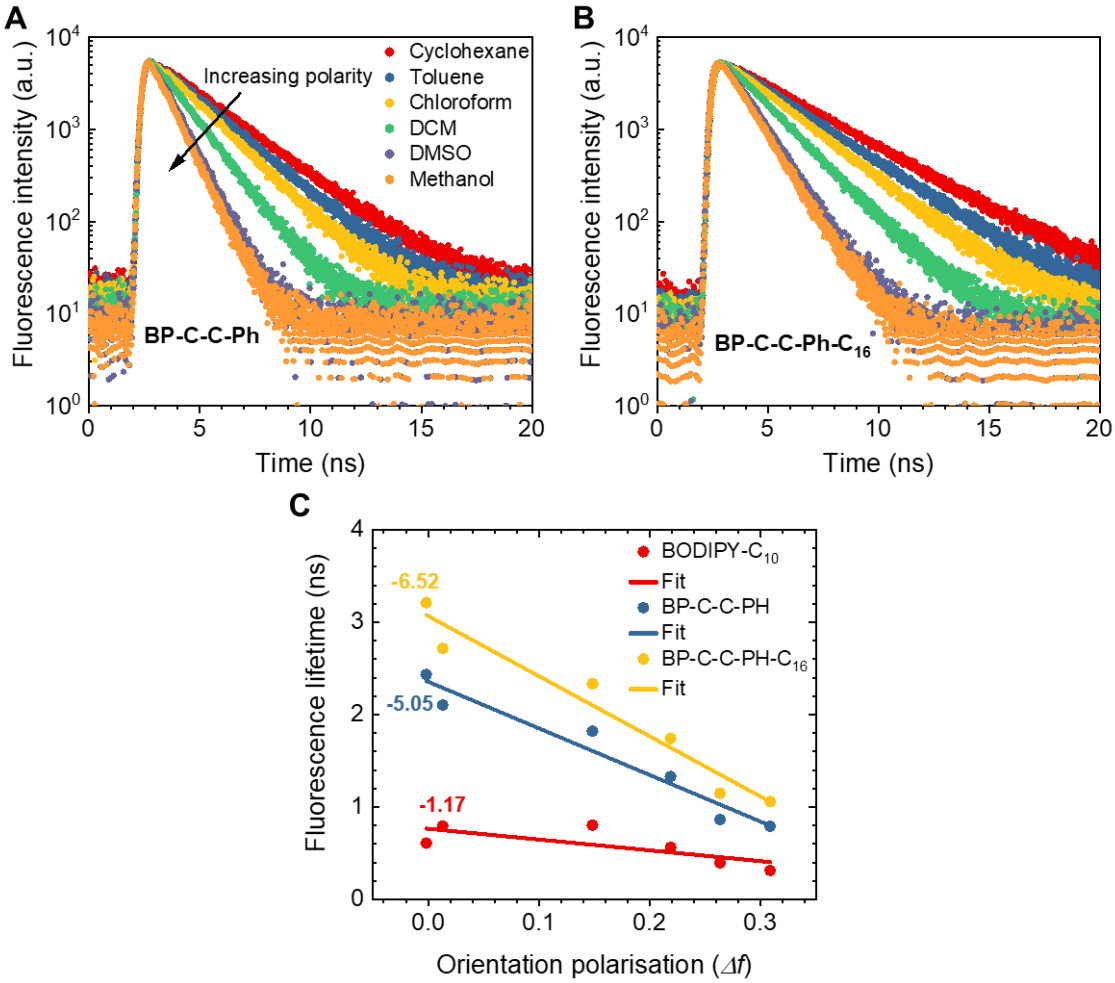

Fig. 25. *Time-resolved fluorescence decays in different polarity solvents of BP-C-C-Ph (A), BP-C-C-Ph-C_{16} (B) and fluorescence lifetimes (C) of BODIPY-C_{10} (red), BP-C-C-Ph (blue), BP-C-C-Ph-C_{16} (yellow) obtained in different solvents with respect to the orientation polarisation of these solvents. Slope values of linear fits are also shown.*

3.2.4 Dependency on solvent temperature

Finally, dependency on solvent temperature was measured. BP-C-C-Ph and BP-C-C-Ph-C_{16} fluorophores showed modest sensitivity to increasing temperature (Fig. 26). Also, it is similar to the temperature sensitivity of BODIPY-C_{10} fluorophore.

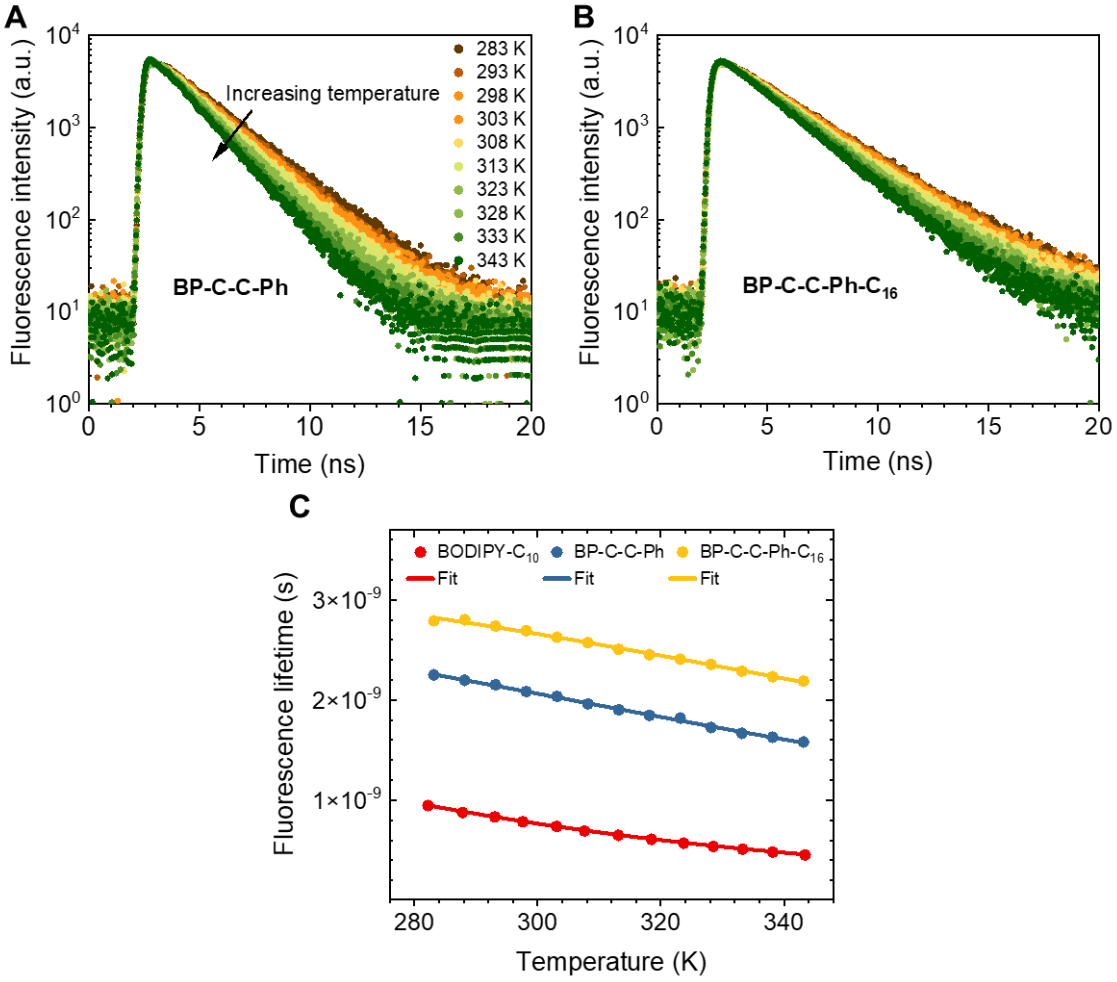

Fig. 26. *Time-resolved fluorescence decays of BP-C-C-Ph (A), BP-C-C-Ph-C_{16} (B) and fluorescence lifetimes (C) BODIPY-C_{10} (red), BP-C-C-Ph (blue), BP-C-C-Ph-C_{16} (yellow) obtained in toluene at different temperatures.*

Experimental values of the sum of radiative and all temperature-independent non-radiative decay rates (k_x), maximum temperature-dependent decay rate ($k_{nr,max}$) and activation energy (E_a) of BODIPY-C_{10}, BP-C-C-Ph and BP-C-C-Ph-C_{16} molecules in toluene are shown in Table 5. Values were obtained after fitting temperature-dependent lifetimes with Eq. 15. Addition of EDG increased energy barrier by 12 meV.

Table 5. *Experimental values of the sum of radiative and all temperature-independent non-radiative decay rates (k_x), maximum temperature-dependent decay rate ($k_{nr,max}$) and activation energy (E_a) of BODIPY-C_{10}, BP-C-C-Ph and BP-C-C-Ph-C_{16} molecules in toluene.*

Molecule	k_x, ns^{-1}	$k_{nr,max}$, ns^{-1}	E_a, meV
BODIPY-C_{10}	0.50±0.03	290±47	152±5
BP-C-C-Ph	0.34±0.02	46±24	149±17
BP-C-C-Ph-C_{16}	0.31±0.01	35±26	161±23

3.3 BP-Ph fluorophores

The final group of this work is the biggest and consists of six fluorophores (Fig. 27). BP-Ph molecule has three phenyl substituents attached to 2-, 6- and 8- position of BODIPY core molecule. Next five fluorophores can be divided into two subgroups. First subgroup is BP-Ph-mMethyl molecules which have four *meta*-methyl substituents and *meso*-phenyl substituent which is unsubstituted for BP-Ph-mMethyl or has either alkoxy (-$OC_{16}H_{33}$) or nitro (-NO_2) substituent on para position of the ring respectively for BP-Ph-mMethyl-C_{16} and BP-Ph-mMethyl-NO_2. Molecules of the second subgroup have the same methyl substituents but in *ortho* position. And as well are unsubstituted at *meso*-phenyl ring for BP-Ph-oMethyl or has nitro (-NO_2) substituent on para position of the ring (BP-Ph-oMethyl-NO_2). *β*-phenyl moieties were added to BODIPY molecule to extend π-conjugation as with previous groups of fluorophores. Different position (*meta* or *ortho*) of methyl substituents were chosen to check the role of steric factors on the sensitivity of the fluorophores.

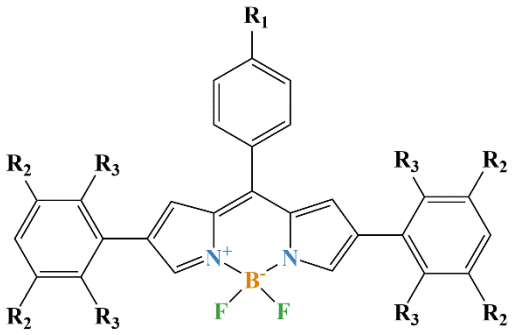

BP-Ph	$R_{1,2,3}$ = -H
BP-Ph-mMethyl	$R_{1,3}$ = -H, R_2 = -CH_3
BP-Ph-mMethyl-C_{16}	R_1 = -$OC_{16}H_{33}$, R_2 = -CH_3, R_3 = -H
BP-Ph-mMethyl-NO_2	R_1 = -NO_2, R_2 = -CH_3, R_3 = -H
BP-Ph-oMethyl	$R_{1,2}$ = -H, R_3 = -CH_3
BP-Ph-oMethyl-NO_2	R_1 = -NO_2, R_2 = -H, R_3 = -CH_3

Fig. 27. *The molecular structures of BODIPY derivatives (BP-Ph, BP-Ph-mMethyl, BP-Ph-mMethyl-C_{16}, BP-Ph-mMethyl-NO_2, BP-Ph-oMethyl, BP-Ph-oMethyl-NO_2).*

3.3.1 Absorption and fluorescence spectra

The absorption spectra of BP-Ph molecules consist of the main absorption band at 520–560 nm (BP-Ph-oMethyl and BP-Ph-oMethyl-NO_2) or 580–620 nm (BP-Ph, BP-Ph-mMethyl, BP-Ph-mMethyl-C_{16}, BP-Ph-mMethyl-NO_2), and a higher energy band located at 350–450 nm (Fig. 28A). Compared to BODIPY-C_{10}, BP-Ph absorption spectrum is red-shifted by 89 nm due to increased conjugation. Addition of methyl substituents to the *ortho* position of *β*-phenyls increased steric hindrance. BP-Ph-oMethyl and BP-Ph-oMethyl-NO_2 absorption maximum is at 530 nm and 545 nm, respectively. Hipsochromic shift is a result of prevented conjugation between the BODIPY core and *β*-phenyls. Change of methyl groups position, from *ortho* to *meta*, eliminated steric factors and absorption spectrum of BP-Ph-mMethyl was red-shifted by 70 nm compared to BP-Ph-oMethyl. Addition of alkoxy group with sixteen carbon atoms resulted in 5 nm shift towards blue part for BP-Ph-mMethyl-C_{16} fluorophore. While addition of nitro group shifted absorption maximum by 15 nm towards red part of the visible spectrum. Similar trends are seen in the fluorescence spectra as well (Fig. 28B). BP-Ph fluorescence emission maximum is located at 630 nm with Stokes shift of 1076 cm^{-1}. BP-Ph-oMethyl and BP-Ph-oMethyl-NO_2 maximum and Stokes shift values are 585 nm

(1774 cm^{-1}) and 620 nm (2220 cm^{-1}), respectively. Absorption, fluorescence maximum values and Stokes shifts for BP-Ph-mMethyl, BP-Ph-mMethyl-C_{16} and BP-Ph-mMethyl-NO_2 molecules are 642 nm (1090 cm^{-1}), 633 nm (1009 cm^{-1}), and 679 nm (1533 cm^{-1}).

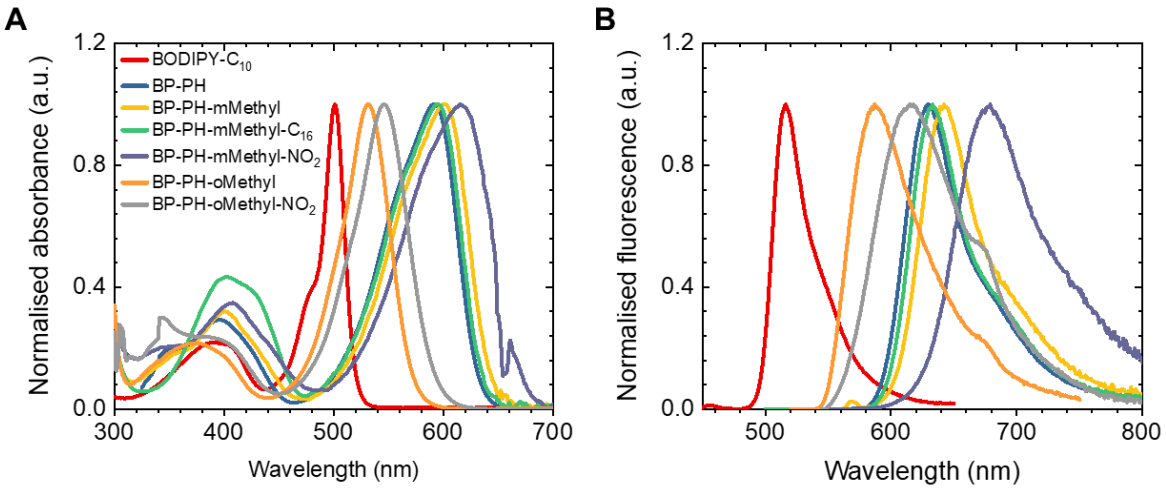

Fig. 28. *Absorption and fluorescence spectra of BP-Ph (blue), BP-Ph-mMethyl (yellow), BP-Ph-mMethyl-C_{16} (green), BP-Ph-mMethyl-NO_2 (violet), BP-Ph-oMethyl (orange), BP-Ph-oMethyl-NO_2 (grey) molecules compared to BODIPY-C_{10} (red) molecular rotor in toluene.*

Experimental values of absorption (λ_{Abs}) and fluorescence (λ_{Fl}) maximum, Stokes shifts (ν_S) and molar extinction coefficients (ε_e) of BODIPY-C_{10}, BP-Ph, BP-Ph-mMethyl, BP-Ph-mMethyl-C_{16}, BP-Ph-mMethyl-NO_2, BP-Ph-oMethyl and BP-Ph-oMethyl-NO_2 molecules in toluene are presented in Table 6.

Table 6. Experimental values of absorption (λ_{Abs}) and fluorescence (λ_{Fl}) maximum, Stokes shifts (ν_S) and molar extinction coefficients (ε_e) of BODIPY-C_{10}, BP-Ph, BP-Ph-mMethyl, BP-Ph-mMethyl-C_{16}, BP-Ph-mMethyl-NO_2, BP-Ph-oMethyl and BP-Ph-oMethyl-NO_2 molecules in toluene.

Molecule	**λ_{Abs}, nm**	**λ_{Fl}, nm**	**ν_S, cm^{-1}**	**ε_e, $M^{-1}\cdot cm^{-1}$**
BODIPY-C_{10}	501	516	580	$6.4\cdot10^4$
BP-Ph	590	630	1076	$3.3\cdot10^4$
BP-Ph-mMethyl	600	642	1090	$4.4\cdot10^4$
BP-Ph-mMethyl-C_{16}	595	633	1009	$4.4\cdot10^4$
BP-Ph-mMethyl-NO_2	615	679	1533	$4.0\cdot10^4$
BP-Ph-oMethyl	530	585	1774	$3.3\cdot10^4$
BP-Ph-oMethyl-NO_2	545	620	2220	$6.5\cdot10^4$

3.3.2 Dependency on solvent viscosity

First of all, as with all previous dyes dependency on solvent viscosity was assessed. Biexponential decays were obtained only in castor oil owing to its small autofluorescence. Viscosity sensitivity of fluorophores is depicted in Fig. 29. BP-Ph-mMethyl-C_{16} molecule was insoluble in glycerol, thus no corresponding fluorescence decay is shown (Fig. 29C). Almost no sensitivity to viscosity were seen for BP-Ph, BP-Ph-mMethyl, BP-Ph-mMethyl-C_{16} and BP-Ph-oMethyl as their lifetimes increased only by 38 % (from 3.14 to 4.32 ns), 26 % (from 3.13 to 3.95 ns), 17 % (from 3.96 to 4.65 ns) and 63 % (from 2.78 to 4.53 ns). All BP-Ph derivatives showed low *x*

values (0.04, 0.03, 0.02 and 0.07 respectively) from Förster-Hoffmann fits. BP-Ph-mMethyl-NO_2 similarly to BP-Vinyl-NO_2 showed approximately three times longer fluorescence decay time in viscous non-polar castor oil solvent in contrast to non-viscous non-polar toluene solvent. *x* value for BP-Ph-mMethyl-NO_2 increased four times which coincides with increased viscosity sensitivity. Nevertheless, sensitivity to viscosity of BP-Ph-mMethyl-NO_2 was lower compared to BODIPY-C_{10}. BP-Ph-oMethyl-NO_2 fluorophore exhibit the strongest viscosity sensitivity of all discussed molecules. Its lifetime increased by 361 % (from 0.53 to 2.43 ns), *x* value from Förster-Hoffmann fit was 0.23. BP-Ph-oMethyl-NO_2 sensitivity is similar to BODIPY-C_{10} molecule while lifetime values are shorter. Steric factors of methyl substituents in the *ortho* position of *β*-phenyls limits large-amplitude motions. Thus, rotation is slower in viscous environment and time the molecules spend in excited state is prolonged compared to the molecule with methyl groups in *meta* position. Among all six BP-Ph molecules both nitro-substituted molecules (BP-Ph-mMethyl-NO_2 and BP-Ph-oMethyl-NO_2) could be used as viscosity sensors.

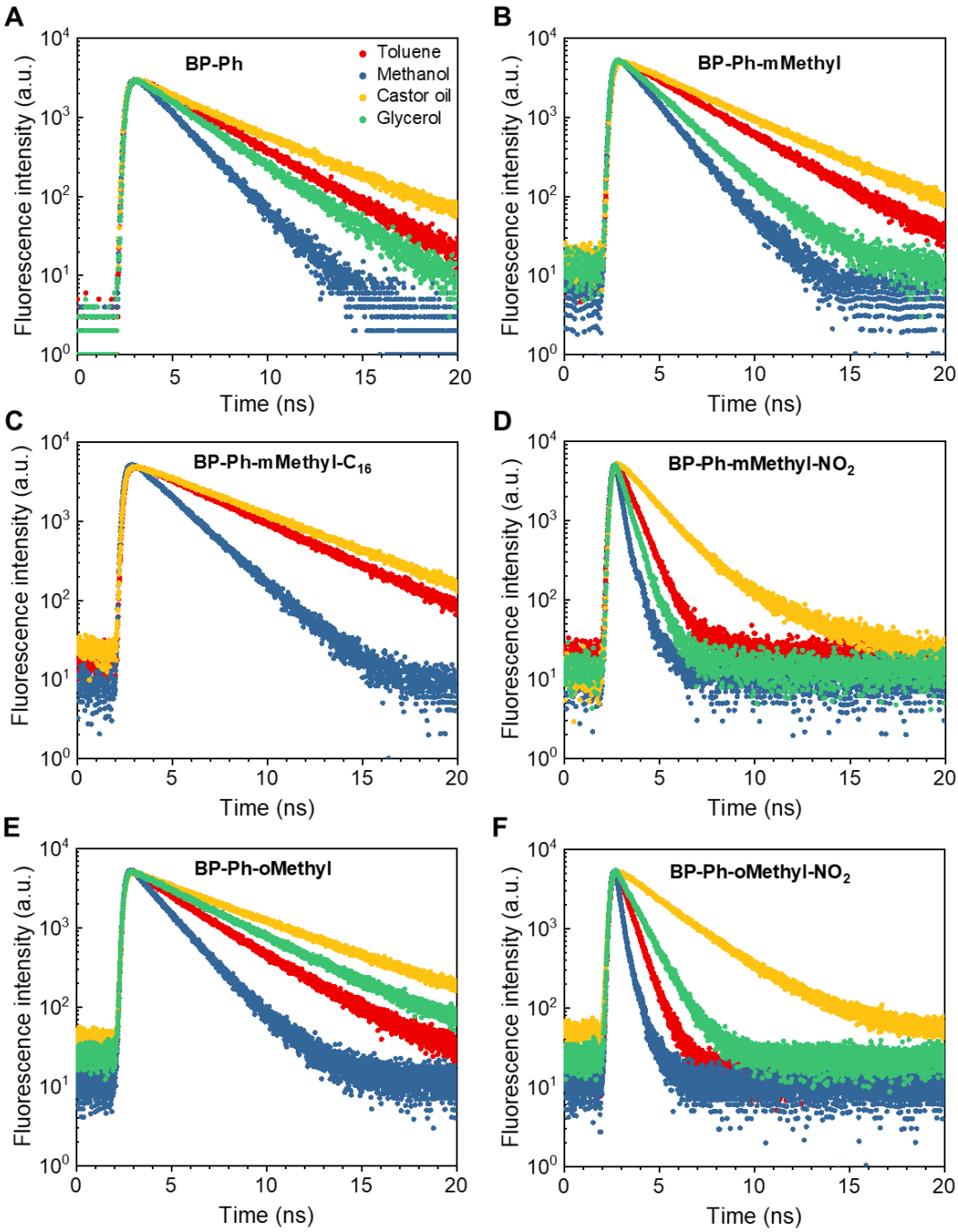

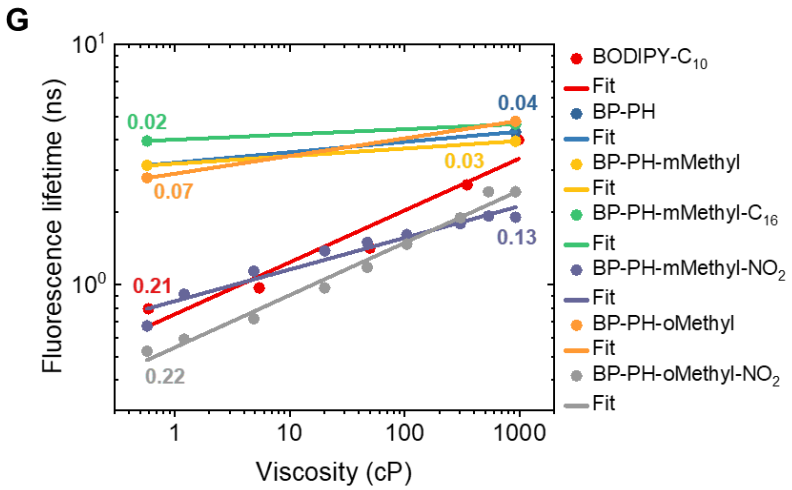

Fig. 29. *Time-resolved fluorescence decays in different viscosity solvents of BP-Ph (A), BP-Ph-mMethyl (B), BP-Ph-mMethyl-C_{16} (C), BP-Ph-mMethyl-NO_2 (D), BP-Ph-oMethyl (E), BP-Ph-oMethyl-NO_2 (F) and fluorescence lifetimes (G) of BP-Ph (blue), BP-Ph-mMethyl (yellow), BP-Ph-mMethyl-C_{16} (green), BP-Ph-mMethyl-NO_2 (violet), BP-Ph-oMethyl (orange), BP-Ph-oMethyl-NO_2 (grey) obtained in different solvents with respect to the viscosity of these solvents. x values from fitting with Eq. 18 that show the extent of viscosity sensitivity are also shown.*

3.3.3 Dependency on solvent polarity

Secondly, polarity sensitivity of BP-Ph fluorophores was determined. As seen previously, polarity of solvent did not have significant impact on their absorption and fluorescence spectra. Absorption maximum changed only by 5 nm at most. While fluorescence maximum peak value varied around 13–25 nm (from cyclohexane to DMSO). Lifetime values of all six fluorophores decreased with increasing polarity (Fig. 30).

BP-Ph, BP-Ph-mMethyl and BP-Ph-oMethyl showed similar sensitivity to the polarity of solvent in 3–5 ns time range. Alkoxy-substituted BP-Ph-mMethyl-C_{16} dye showed the strongest dependency to polarity with gradually decreasing lifetime values with increasing solvent polarity. Therefore, it could be used as polarity sensor. Addition of electron withdrawing nitro group suppressed sensitivity to polarity 2.5 and 4 times for BP-Ph-mMethyl-NO_2 and BP-Ph-oMethyl-NO_2, respectively. The same sensitivity suppression was seen before with BP-Vinyl-NO_2 molecule. Compared to the BODIPY-C_{10} lifetime values were in the same 0.5–1 ns time range.

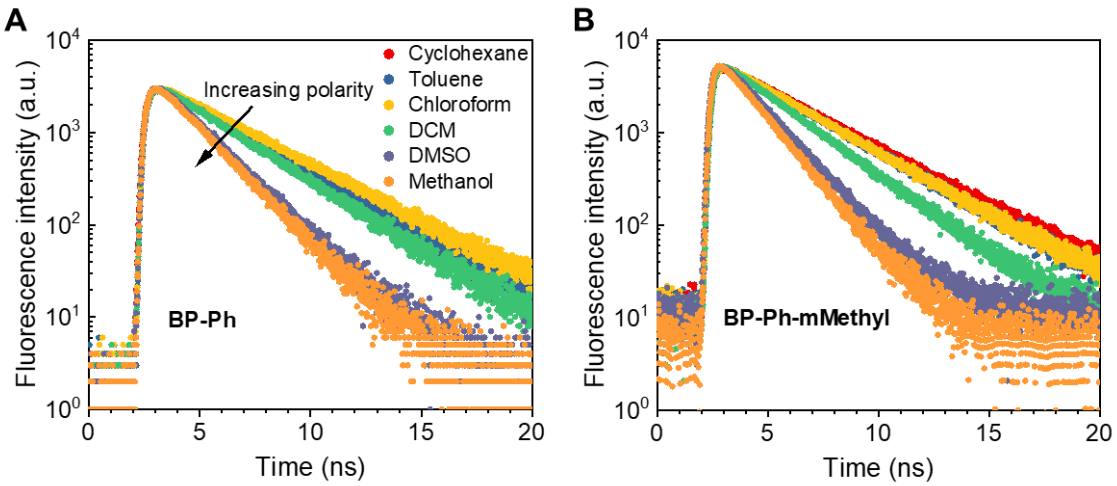

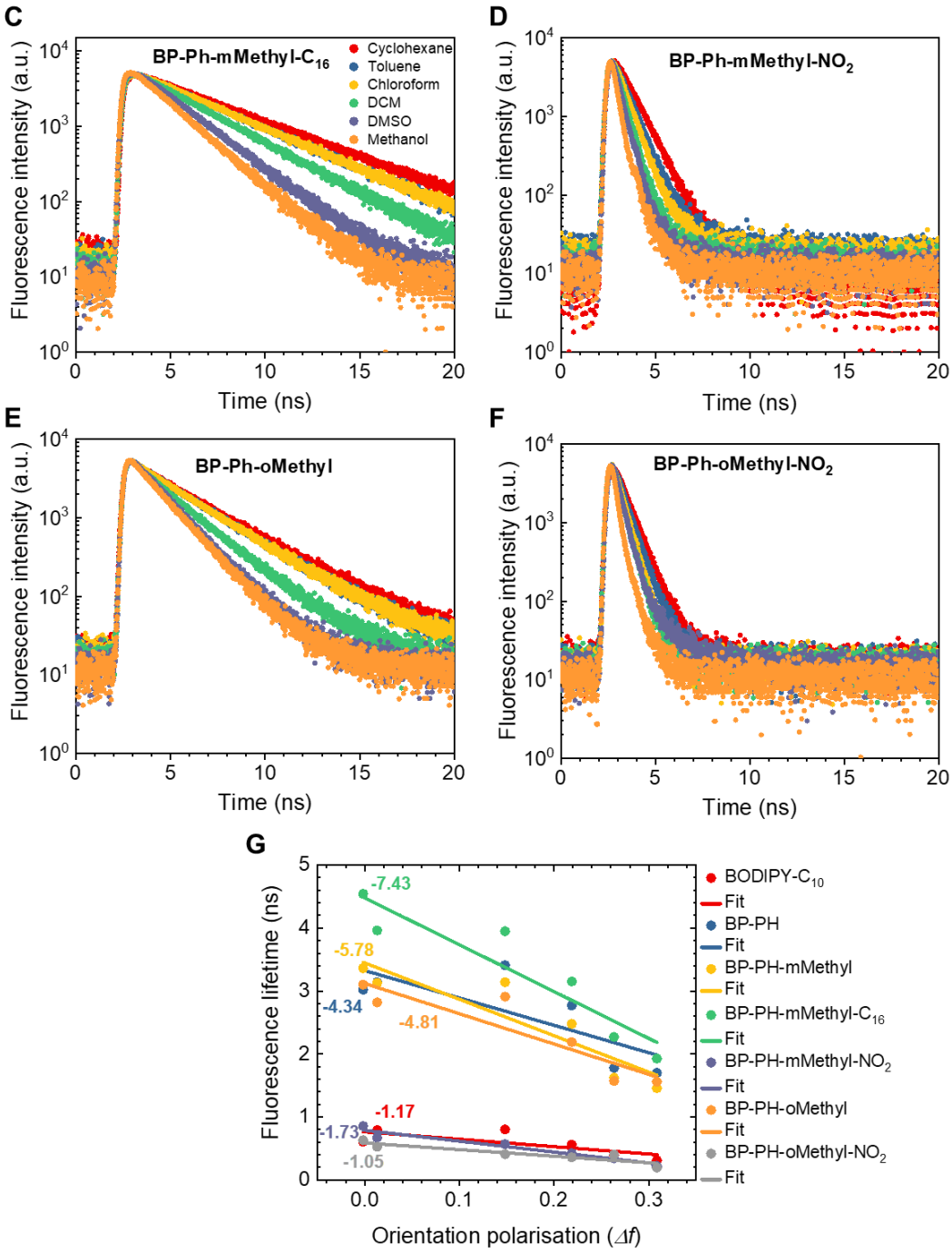

Fig. 30. *Time-resolved fluorescence decays in different polarity solvents of BP-Ph (A), BP-Ph-mMethyl (B), BP-Ph-mMethyl-C_{16} (C), BP-Ph-mMethyl-NO_2 (D), BP-Ph-oMethyl (E), BP-Ph-oMethyl-NO_2 (F) and fluorescence lifetimes (G) of BP-Ph (blue), BP-Ph-mMethyl (yellow), BP-Ph-mMethyl-C_{16} (green), BP-Ph-mMethyl-NO_2 (violet), BP-Ph-oMethyl (orange), BP-Ph-oMethyl-C_{16} (grey) obtained in different solvents with respect to the orientation polarisation of these solvents. Slope values of linear fits are also shown.*

3.3.4 Dependency on solvent temperature

Finally, all the six molecules showed modest sensitivity to increasing temperature (Fig. 31). Also, it is similar to the temperature sensitivity of BODIPY-C_{10} fluorophore. BP-Ph-mMethyl-NO_2 and BP-Ph-oMethyl-NO_2 had very short lifetime values which is similar to BODIPY-C_{10} lifetime values.

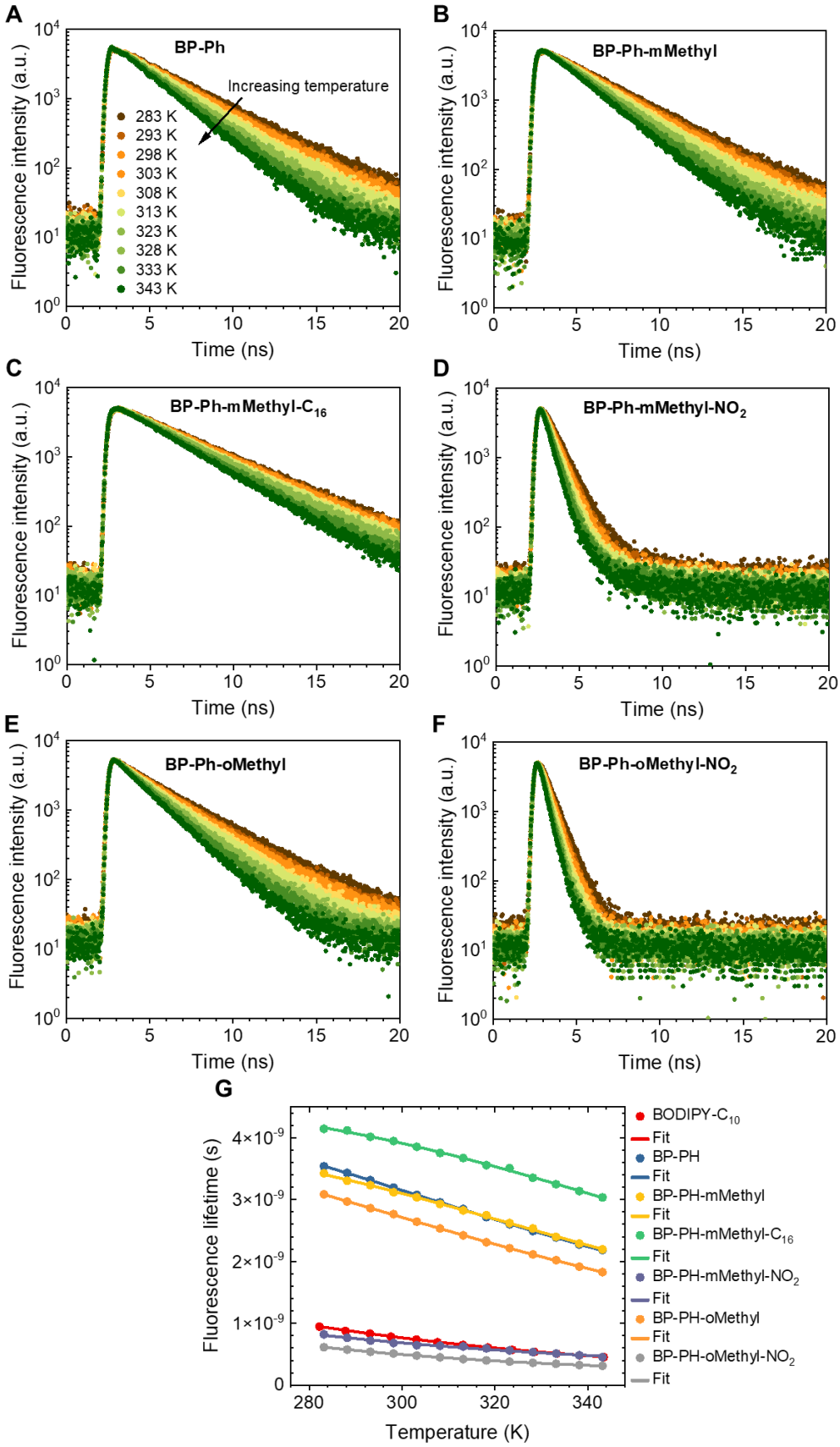

Fig. 31. *Time-resolved fluorescence decays of BP-Ph (A), BP-Ph-mMethyl (B), BP-Ph-mMethyl-C_{16} (C), BP-Ph-mMethyl-NO_2 (D), BP-Ph-oMethyl (E), BP-Ph-oMethyl-NO_2 (F) and fluorescence lifetimes (G) of BP-Ph (blue), BP-Ph-mMethyl (yellow), BP-Ph-mMethyl-C_{16} (green), BP-Ph-mMethyl-NO_2 (violet), BP-Ph-oMethyl (orange), BP-Ph-oMethyl-C_{16} (grey) obtained in toluene at different temperatures.*

Experimental values of the sum of radiative and all temperature-independent non-radiative decay rates (k_x), maximum temperature-dependent decay rate ($k_{nr,max}$) and activation energy values (E_a) of BODIPY-C_{10}, BP-Ph-mMethyl, BP-Ph-mMethyl-C_{16}, BP-Ph-mMethyl-NO_2, BP-Ph-oMethyl, BP-Ph-oMethyl-NO_2 molecules in toluene are shown in Table 7. Values were obtained after fitting temperature-dependent lifetimes with Eq. 15. Compared to BP-Ph energy barrier values were lowered by 78 meV and 70 meV for nitro-substituted fluorophores. The value was more than 50 meV lower compared to BODIPY-C_{10} molecule, which explains good viscosity sensitivity. BP-Ph-mMethyl-C_{16} stood out among all molecules with biggest value of E_a=220 meV.

Table 7. *Experimental values of the sum of radiative and all temperature-independent non-radiative decay rates (k_x), maximum temperature-dependent decay rate ($k_{nr,max}$) and activation energy (E_a) of BODIPY-C_{10}, BP-Ph-mMethyl, BP-Ph-mMethyl-C_{16}, BP-Ph-mMethyl-NO_2, BP-Ph-oMethyl, BP-Ph-oMethyl-NO_2 molecules in toluene.*

Molecule	k_x, ns^{-1}	$k_{nr,max}$, ns^{-1}	E_a, meV
BODIPY-C_{10}	0.50±0.03	290±47	152±5
BP-Ph	0.21±0.01	90±11	174±4
BP-Ph-mMethyl	0.25±0.01	215±88	205±13
BP-Ph-mMethyl-C_{16}	0.22±0.01	193±101	220±16
BP-Ph-mMethyl-NO_2	0.33±0.04	46±5	96±37
BP-Ph-oMethyl	0.23±0.01	112±16	174±5
BP-Ph-oMethyl-NO_2	0.18±0.01	102±20	104±7

CONCLUSIONS

1. New BODIPY-based fluorescent molecular rotors were characterised and it was assessed how changes in the molecular structure influence their spectroscopic properties and sensitivity to the viscosity, polarity, and temperature of the environment.

2. Compared to widely used BODIPY-C_{10} molecular rotor, prolonged conjugated system in the new molecules resulted in bathochromic shift in both absorption and fluorescence emission spectra.

3. Adding electron donating alkoxy (-$OC_{16}H_{33}$) substituent did not have any impact on viscosity sensitivity. Nonetheless both BP-C-C-Ph-C_{16} and BP-Ph-mMethyl-C_{16} could be used to sense polarity.

4. Adding electron withdrawing nitro (-NO_2) group is a universal method to increase sensitivity of the molecule to the viscosity of a medium. Three new microviscosity probes (BP-Vinyl-NO_2, BP-Ph-mMethyl-NO_2, BP-Ph-oMethyl-NO_2) were successfully investigated. Furthermore, it was shown that BP-Vinyl-NO_2 fluorophore could be used to probe high microviscosity environments.

5. Steric hindrance in the molecules resulted in hipsochromic shift in absorption and fluorescence emission spectra due to prevented conjugation between the BODIPY core and *β*-phenyls. On the other hand, it increased viscosity sensitivity by slowing rotation of the molecular rotor in viscous environment.

LITERATURE

[1] M.K. Kuimova, Mapping viscosity in cells using molecular rotors, Physical Chemistry Chemical Physics. 14 (2012) 12671–12686. https://doi.org/10.1039/C2CP41674C.

[2] M. Shinitzky, Membrane fluidity in malignancy Adversative and recuperative, Biochimica et Biophysica Acta (BBA) - Reviews on Cancer. 738 (1984) 251–261. https://doi.org/10.1016/0304-419X(83)90007-0.

[3] O. Nadiv, M. Shinitzky, H. Manu, D. Hecht, C.T. Roberts, D. LeRoith, Y. Zick, Elevated protein tyrosine phosphatase activity and increased membrane viscosity are associated with impaired activation of the insulin receptor kinase in old rats., Biochemical Journal. 298 (1994) 443. https://doi.org/10.1042/BJ2980443.

[4] Z. Yang, J. Cao, Y. He, J.H. Yang, T. Kim, X. Peng, J.S. Kim, Macro-/micro-environment-sensitive chemosensing and biological imaging, Chem. Soc. Rev. 43 (2014) 4563. https://doi.org/10.1039/c4cs00051j.

[5] A. Vyšniauskas, M.K. Kuimova, A twisted tale: Measuring viscosity and temperature of microenvironments using molecular rotors, International Reviews in Physical Chemistry. 37 (2018) 259–285. https://doi.org/10.1080/0144235X.2018.1510461.

[6] S.C. Lee, J. Heo, H.C. Woo, J.A. Lee, Y.H. Seo, C.L. Lee, S. Kim, O.P. Kwon, Fluorescent Molecular Rotors for Viscosity Sensors, Chemistry - A European Journal. 24 (2018) 13706–13718. https://doi.org/10.1002/CHEM.201801389.

[7] S. Toliautas, J. Dodonova, A. Žvirblis, I. Čiplys, A. Polita, A. Devižis, S. Tumkevičius, J. Šulskus, A. Vyšniauskas, Enhancing the Viscosity-Sensitive Range of a BODIPY Molecular Rotor by Two Orders of Magnitude, Chemistry - A European Journal. 25 (2019) 10342–10349. https://doi.org/10.1002/chem.201901315.

[8] B. Valeur, Molecular Fluorescence: Principles and Applications, Wiley-VCH Verlag GmbH, 2001.

[9] Viscosity - Wikipedia, (n.d.). https://en.wikipedia.org/wiki/Viscosity (accessed April 26, 2022).

[10] R.J. Silbey, R.A. Alberty, M.G. Bawendi, Physical Chemistry, 4th Edition, JohnWiley&Sons,Inc., 2004.

[11] P. Atkins, J. de Paula, Physical Chemistry, 10th Edition, Oxford University Press, 2006.

[12] M.A. Haidekker, E.A. Theodorakis, Molecular rotors - Fluorescent biosensors for viscosity and flow, Organic and Biomolecular Chemistry. 5 (2007) 1669–1678. https://doi.org/10.1039/b618415d.

[13] O. Nadiv, M. Shinitzky, H. Manu, D. Hecht, C.T. Roberts, D. LeRoith, Y. Zick, Elevated protein tyrosine phosphatase activity and increased membrane viscosity are associated with impaired activation of the insulin receptor kinase in old rats, Biochemical Journal. 298 (1994) 443–450. https://doi.org/10.1042/BJ2980443.

[14] C. Irace, C. Carallo, F. Scavelli, M.S. de Franceschi, T. Esposito, A. Gnasso, Blood Viscosity in Subjects With Normoglycemia and Prediabetes, Diabetes Care. 37 (2014) 488–492. https://doi.org/10.2337/DC13-1374.

[15] G. Deliconstantinos, V. Villiotou, J.C. Stavrides, Modulation of particulate nitric oxide synthase activity and peroxynitrite synthesis in cholesterol enriched endothelial cell membranes, Biochemical Pharmacology. 49 (1995) 1589–1600. https://doi.org/10.1016/0006-2952(95)00094-G.

[16] G.S. Zubenko, B.M. Cohen, C.F. Reynolds, F. Boller, I. Malinakova, N. Keefe, Platelet membrane fluidity in Alzheimer's disease and major depression, American Journal of Psychiatry. 144 (1987) 860–868. https://doi.org/10.1176/AJP.144.7.860.

[17] J. Li, Y. Zhang, H. Zhang, X. Xuan, M. Xie, S. Xia, G. Qu, H. Guo, Nucleoside-Based Ultrasensitive Fluorescent Probe for the Dual-Mode Imaging of Microviscosity in Living Cells, Analytical Chemistry. 88 (2016) 5554–5560. https://doi.org/https://doi.org/10.1021/acs.analchem.6b01395.

[18] D.L., Pavia, G.M., Lampman, G.S. Kriz, Introduction to spectroscopy: A guide for students of organic chemistry, 3rd ed., W.B. Saunders Co. , Philadelphia, 1979.

[19] W.S. Price, P.W. Kuchel, B.A. Cornell, Microviscosity of human erythrocytes studied with hypophosphite and 31P-NMR, Biophysical Chemistry. 33 (1989) 205–215. https://doi.org/10.1016/0301-4622(89)80022-5.

[20] Y. Ye, X. Liu, Z. Zhang, Q. Wu, B. Jiang, L. Jiang, X. Zhang, M. Liu, G.J. Pielak, C. Li, 19F NMR spectroscopy as a probe of cytoplasmic viscosity and weak protein interactions in living cells, Chemistry - A European Journal. 19 (2013) 12705–12710. https://doi.org/10.1002/CHEM.201301657.

[21] CRC Handbook of Chemistry and Physics, CRC Press, 2016. https://doi.org/10.1201/9781315380476.

[22] D. Goldfarb, S. Stoll, EPR Spectroscopy: Fundamentals and Methods, JohnWiley&Sons,Inc., 2018.

[23] S. Siepe, W. Herrmann, H.H. Borchert, B. Lueckel, A. Kramer, A. Ries, R. Gurny, Microenvironmental pH and microviscosity inside pH-controlled matrix tablets: An EPR imaging study, Journal of Controlled Release. 112 (2006) 72–78. https://doi.org/10.1016/J.JCONREL.2005.12.021.

[24] M. Velayutham, M. Poncelet, T.D. Eubank, B. Driesschaert, V. v. Khramtsov, Biological Applications of Electron Paramagnetic Resonance Viscometry Using a 13C-Labeled Trityl Spin Probe, Molecules 2021, Vol. 26, Page 2781. 26 (2021) 2781. https://doi.org/10.3390/MOLECULES26092781.

[25] A. Carisey, M. Stroud, R. Tsang, C. Ballestrem, Fluorescence Recovery After Photobleaching, Humana Press, 2011. https://doi.org/10.1007/978-1-61779-207-6_26.

[26] E.A.J. Reits, J.J. Neefjes, From fixed to FRAP: Measuring protein mobility and activity in living cells, Nature Cell Biology. 3 (2001). https://doi.org/10.1038/35078615.

[27] L.B. Persson, V.S. Ambati, O. Brandman, Cellular Control of Viscosity Counters Changes in Temperature and Energy Availability, Cell. 183 (2020) 1572-1585.e16. https://doi.org/https://doi.org/10.1016/j.cell.2020.10.017.

[28] Practical Manual for Fluorescence Microscopy Techniques | PicoQuant, (n.d.). https://www.picoquant.com/scientific/practical-manual-for-fluorescence-microscopy (accessed April 28, 2022).

[29] N.L. Thompson, Fluorescence Correlation Spectroscopy, Springer, Boston, MA, Boston, 2002. https://doi.org/10.1007/0-306-47057-8_6.

[30] J. Korlach, P. Schwille, W.W. Webb, G.W. Feigenson, Characterization of lipid bilayer phases by confocal microscopy and fluorescence correlation spectroscopy, Proc Natl Acad Sci U S A. 96 (1999) 8461–8466. https://doi.org/https://doi.org/10.1073/pnas.96.15.8461.

[31] J.J. Hung, W.F. Zeno, A.A. Chowdhury, B.J. Dear, K. Ramachandran, M.P. Nieto, T.Y. Shay, C.A. Karouta, C.C. Hayden, J.K. Cheung, T.M. Truskett, J.C. Stachowiak, K.P. Johnston, Self-diffusion of a highly concentrated monoclonal antibody by fluorescence correlation

spectroscopy: insight into protein-protein interactions and self-association, Cite This: Soft Matter. 15 (2019) 6660. https://doi.org/10.1039/c9sm01071h.

[32] J.F. Eccleston, J.P. Hutchinson, D.M. Jameson, Fluorescence-Based Assays, in: Progress in Medicinal Chemistry, Elsevier, 2005: pp. 19–48. https://doi.org/10.1016/S0079-6468(05)43002-7.

[33] C.A. Royer, S.F. Scarlata, Chapter 5 Fluorescence Approaches to Quantifying Biomolecular Interactions, in: Methods in Enzymology, Academic Press, 2008: pp. 79–106. https://doi.org/10.1016/S0076-6879(08)03405-8.

[34] T. Araiso, T. Koyama, A new analysis method for the membrane viscosity from steady-state fluorescence depolarization, Biorheology. 25 (1988) 253–259. https://doi.org/10.3233/BIR-1988-251-234.

[35] R. Kuriyama, T. Nakagawa, K. Tatsumi, K. Nakabe, Two-dimensional fluid viscosity measurement in microchannel flow using fluorescence polarization imaging, Measurement Science and Technology. 32 (2021) 095402. https://doi.org/10.1088/1361-6501/ABECCB.

[36] W. Zheng, D. Li, J.Y. Qu, Monitoring changes of cellular metabolism and microviscosity in vitro based on time-resolved endogenous fluorescence and its anisotropy decay dynamics, (2010). https://doi.org/10.1117/1.3449577.

[37] H.A. Kramers, Brownian motion in a field of force and the diffusion model of chemical reactions, Physica. 7 (1940) 284–304. https://doi.org/10.1016/S0031-8914(40)90098-2.

[38] T. Förster, G. Hoffmann, Die Viskositätsabhängigkeit der Fluoreszenzquantenausbeuten einiger Farbstoffsysteme, Zeitschrift Fur Physikalische Chemie. 75 (1971) 63–76. https://doi.org/https://doi.org/10.1524/zpch.1971.75.1_2.063.

[39] M.A. Haidekker, N. L'Heureux, J.A. Frangos, Fluid shear stress increases membrane fluidity in endothelial cells: A study with DCYJ fluorescence, American Journal of Physiology - Heart and Circulatory Physiology. 278 (2000). https://doi.org/https://doi.org/10.1152/ajpheart.2000.278.4.H1401.

[40] C.E. Kung, J.K. Reed, Microviscosity Measurements of Phospholipid Bilayers Using Fluorescent Dyes That Undergo Torsional Relaxation, Biochemistry. 25 (1986) 6114–6121. https://doi.org/https://doi.org/10.1021/bi00368a042.

[41] R.O. Loutfy, Fluorescence probes for polymer free-volume, Pure and Applied Chemistry. 58 (1986) 1239–1248. https://doi.org/https://doi.org/10.1351/pac198658091239.

[42] M.A. Haidekker, T. Ling, M. Anglo, H.Y. Stevens, J.A. Frangos, E.A. Theodorakis, New fluorescent probes for the measurement of cell membrane viscosity, Chemistry & Biology. 8 (2001) 123–131. https://doi.org/10.1016/S1074-5521(00)90061-9.

[43] M.A. Haidekker, T.P. Brady, D. Lichlyter, E.A. Theodorakis, A ratiometric fluorescent viscosity sensor, J Am Chem Soc. 128 (2006) 398–399. https://doi.org/https://doi.org/10.1021/ja056370a.

[44] G. Li, R. Guo, M. Pei, W. Lin, Construction of a novel GQD based ratiometric fluorescent composite probe for viscosity detection, Chemical Communications. 56 (2020) 14649–14652. https://doi.org/10.1039/D0CC05836J.

[45] M.R. Dent, I. López-Duarte, C.J. Dickson, N.D. Geoghegan, J.M. Cooper, I.R. Gould, R. Krams, J.A. Bull, N.J. Brooks, M.K. Kuimova, Imaging phase separation in model lipid membranes through the use of BODIPY based molecular rotors, Physical Chemistry Chemical Physics. 17 (2015) 18393–18402. https://doi.org/10.1039/C5CP01937K.

[46] X. Peng, Z. Yang, J. Wang, J. Fan, Y. He, F. Song, B. Wang, S. Sun, J. Qu, J. Qi, M. Yan, Fluorescence ratiometry and fluorescence lifetime imaging: Using a single molecular sensor

for dual mode imaging of cellular viscosity, J Am Chem Soc. 133 (2011) 6626–6635. https://doi.org/https://doi.org/10.1021/ja1104014.

[47] A. Vyšniauskas, M. Balaz, H.L. Anderson, M.K. Kuimova, Dual mode quantitative imaging of microscopic viscosity using a conjugated porphyrin dimer, Physical Chemistry Chemical Physics. 17 (2015) 7548–7554. https://doi.org/10.1039/C5CP00439J.

[48] A. Treibs, F. -H Kreuzer, Difluorboryl-Komplexe von Di- und Tripyrrylmethenen, Justus Liebigs Ann Chem. 718 (1968) 208–223. https://doi.org/10.1002/JLAC.19687180119.

[49] G. Ulrich, R. Ziessel, A. Harriman, The Chemistry of Fluorescent Bodipy Dyes: Versatility Unsurpassed, Angewandte Chemie International Edition. 47 (2008) 1184–1201. https://doi.org/10.1002/ANIE.200702070.

[50] L. Jean-Gérard, W. Vasseur, F. Scherninski, B. Andrioletti, Recent advances in the synthesis of [a]-benzo-fused BODIPY fluorophores, Chemical Communications. 54 (2018) 12914–12929. https://doi.org/10.1039/C8CC06403B.

[51] A. Loudet, K. Burgess, BODIPY dyes and their derivatives: Syntheses and spectroscopic properties, Chemical Reviews. 107 (2007) 4891–4932. https://doi.org/https://doi.org/10.1021/cr078381n.

[52] K. Maleckaitė, J. Dodonova, S. Toliautas, R. Žilėnaitė, D. Jurgutis, V. Karabanovas, S. Tumkevičius, A. Vyšniauskas, Designing a Red-Emitting Viscosity-Sensitive BODIPY Fluorophore for Intracellular Viscosity Imaging, Chemistry - A European Journal. 27 (2021). https://doi.org/10.1002/chem.202102743.

[53] K. Maleckaitė, D. Narkevičius, R. Žilėnaitė, J. Dodonova-Vaitkūnienė, S. Toliautas, S. Tumkevičius, A. Vyšniauskas, Give or take: Effects of electron-accepting/-withdrawing groups in red-fluorescent BODIPY molecular rotors, Molecules. 27 (2022). https://doi.org/10.3390/molecules27010023.

[54] J.E. Chambers, M. Kubánková, R.G. Huber, I. López-Duarte, E. Avezov, P.J. Bond, S.J. Marciniak, M.K. Kuimova, An Optical Technique for Mapping Microviscosity Dynamics in Cellular Organelles, ACS Nano. 12 (2018) 4398–4407. https://doi.org/https://doi.org/10.1021/acsnano.8b00177.

[55] M. Kubánková, J.E. Chambers, R.G. Huber, P.J. Bond, S.J. Marciniak, M.K. Kuimova, Linker length affects photostability of protein-targeted sensor of cellular microviscosity, Methods and Applications in Fluorescence. 7 (2019) 044004. https://doi.org/10.1088/2050-6120/AB481F.

[56] N.A. Hosny, C. Fitzgerald, A. Vyšniauskas, A. Athanasiadis, T. Berkemeier, N. Uygur, U. Pöschl, M. Shiraiwa, M. Kalberer, F.D. Pope, M.K. Kuimova, Direct imaging of changes in aerosol particle viscosity upon hydration and chemical aging, Chemical Science. 7 (2016) 1357–1367. https://doi.org/10.1039/C5SC02959G.

[57] M.K. Kuimova, G. Yahioglu, J.A. Levitt, K. Suhling, Molecular Rotor Measures Viscosity of Live Cells via Fluorescence Lifetime Imaging, J Am Chem Soc. 130 (2008) 19. https://doi.org/10.1021/ja800570d.

[58] A.S. Kashirina, I. López-Duarte, M. Kubánková, A.A. Gulin, V. v. Dudenkova, S.A. Rodimova, H.G. Torgomyan, E. v. Zagaynova, A. v. Meleshina, M.K. Kuimova, Monitoring membrane viscosity in differentiating stem cells using BODIPY-based molecular rotors and FLIM, Scientific Reports 2020 10:1. 10 (2020) 1–12. https://doi.org/10.1038/s41598-020-70972-5.

[59] J.M. Nölle, C. Jüngst, A. Zumbusch, D. Wöll, Monitoring of viscosity changes during free radical polymerization using fluorescence lifetime measurements, Polymer Chemistry. 5 (2014) 2700–2703. https://doi.org/10.1039/C3PY01684F.

[60] A. Vyšniauskas, I. López-Duarte, N. Duchemin, T.T. Vu, Y. Wu, E.M. Budynina, Y.A. Volkova, E. Peña Cabrera, D.E. Ramírez-Ornelas, M.K. Kuimova, Exploring viscosity, polarity and temperature sensitivity of BODIPY-based molecular rotors, Physical Chemistry Chemical Physics. 19 (2017) 25252–25259. https://doi.org/10.1039/C7CP03571C.

[61] A. Prlj, A. Fabrizio, C. Corminboeuf, Rationalizing fluorescence quenching in meso-BODIPY dyes, Physical Chemistry Chemical Physics. 18 (2016) 32668–32672. https://doi.org/10.1039/C6CP06799A.

[62] X. Liu, W. Chi, Q. Qiao, S. v. Kokate, E.P. Cabrera, Z. Xu, X. Liu, Y.T. Chang, Molecular Mechanism of Viscosity Sensitivity in BODIPY Rotors and Application to Motion-Based Fluorescent Sensors, ACS Sensors. 5 (2020) 731–739. https://doi.org/10.1021/acssensors.9b01951.

[63] J.R. Lakowicz, Principles of fluorescence spectroscopy, Principles of Fluorescence Spectroscopy. (2006) 1–954. https://doi.org/10.1007/978-0-387-46312-4.

ACKNOWLEDGMENTS

First of all, I would like to thank my supervisor dr. Aurimas Vyšniauskas, who has been extremely helpful, encouraging and understanding person. Furthermore, I want to thank PhD student Karolina Maleckaitė for teaching me everything in the beginning and for all advice I have received. In addition, I want to express my deep appreciation for everyone who helped me to write this thesis inside and outside the university.

Parts of data and findings presented in this thesis were acquired by K. Maleckaitė:

1. Fluorescence lifetime measurements in cooled glycerol and methanol-glycerol mixtures of BP-Vinyl-NO_2 molecule.
2. Absorption and fluorescence spectra as well as fluorescence lifetime measurements in various solvents of BP-Ph molecule.

Parts of work reported in this thesis were published in the following scientific papers:

1. Maleckaitė, K., Dodonova, J., Toliautas, S., **Žilėnaitė, R.**, Jurgutis, D., Karabanovas, V., Tumkevičius, S., Vyšniauskas, A. (2021). Designing a Red-Emitting Viscosity-Sensitive BODIPY Fluorophore for Intracellular Viscosity Imaging. *Chemistry - A European Journal*, *27*(67). https://doi.org/10.1002/chem.202102743.
2. Maleckaitė, K., Narkevičius, D., **Žilėnaitė, R.**, Dodonova-Vaitkūnienė, J., Toliautas, S., Tumkevičius, S., Vyšniauskas, A. (2022). Give or take: Effects of electron-accepting/-withdrawing groups in red-fluorescent BODIPY molecular rotors. *Molecules*, *27*(1). https://doi.org/10.3390/molecules27010023.

Parts of work reported in this thesis were presented in the following conferences:

1. Spectroscopic Characterisation of BODIPY-Based New Fluorescent Viscosity Sensors. **Rugilė Žilėnaitė**, Karolina Maleckaitė, Jelena Dodonova, Sigitas Tumkevičius, Aurimas Vyšniauskas. Open Readings, Vilnius, Lithuania, 2021.
2. Spectroscopic Investigation of BODIPY-Based Fluorophores for Sensing Viscosity. **Rugilė Žilėnaitė**, Karolina Maleckaitė, Jelena Dodonova, Sigitas Tumkevičius, Aurimas Vyšniauskas. Advanced Materials and Technologies, Palanga, Lithuania, 2021. *Presentation was awarded with best poster title.*
3. Designing a Viscosity-Sensitive BODIPY Fluorophore For A Live Cell Imaging. Karolina Maleckaitė, Jelena Dodonova, Stepas Toliautas, **Rugilė Žilėnaitė**, Džiugas Jurgutis, Vitalijus Karabanovas, Sigitas Tumkevičius, Aurimas Vyšniauskas. Open Readings, Vilnius, Lietuva, 2021.
4. Red-fluorescing BODIPY-based polarity sensor. Karolina Maleckaitė, Jelena Dodonova, **Rugilė Žilėnaitė**, Sigitas Tumkevičius, Aurimas Vyšniauskas. Advanced Materials and Technologies, Palanga, Lietuva, 2021

5. The Impact of Electron-Donating/-Withdrawing Groups On Red-Fluorescent BODIPY Molecular Rotor. Karolina Maleckaitė, Domantas Narkevičius, **Rugilė Žilėnaitė**, Jelena Dodonova-Vaitkūnienė, Stepas Toliautas, Sigitas Tumkevičius, Aurimas Vyšniauskas. Open Readings, Vilnius, Lietuva, 2022.

6. Red-fluorescent BODIPY microviscosity sensor for intracellular imaging. Karolina Maleckaitė, Jelena Dodonova-Vaitkūnienė, Stepas Toliautas, **Rugilė Žilėnaitė**, Džiugas Jurgutis, Vitalijus Karabanovas, Sigitas Tumkevičius, Aurimas Vyšniauskas. Bio-Sensing Technology, Sitges, Ispanija, 2022.

SANTRAUKA

VILNIAUS UNIVERSITETAS
CHEMIJOS IR GEOMOKSLŲ FAKULTETAS

RUGILĖ ŽILĖNAITĖ

Naujų fluorescuojančių klampos jutiklių paremtų BODIPY grupe charakterizavimas spektroskopiniais metodais

Mikroklampa yra vienas iš svarbiausių parametrų biologinėse sistemose mikroskopiniame lygmenyje. Ji gali nulemti difuzijos veikiamų procesų greitį ir tarpląstelines molekulines sąveikas. Mikroklampos vaizdinimas biosistemose suteikia informacijos apie pokyčius ląstelėse ir ligų vystymąsi. Vienas iš patogiausių būdų tai atlikti yra mikroklampai jautrių fluoroforų naudojimas. Fluorescenciniai molekuliniai rotoriai (FMR) – tai organiniai fluoroforai, kurių liuminescencija yra jautri terpės klampai. Sužadinus FMR įvyksta vidumolekulinė rotacija. Mažos klampos tirpikliuose, molekulės vidinė rotacija yra greita. To pasekmė – nespindulinė relaksacija, fluorescencijos gesinimas. Klampiuose tirpikliuose molekulės yra stipriau įmobilizuotos, rotacija sulėtėja, o fluorescencijos intensyvumas išauga. Taip pat išauga fluorescencijos kvantinis našumas bei gyvavimo trukmė.

Vienas iš plačiausiai naudojamų molekulinių rotorių yra boro-dipirometenu (BODIPY) paremtas BODIPY-C_{10} molekulinis rotorius. BODIPY-C_{10} ir kiti panašūs FMR pasižymi lengvu funkcionalizavimu, fotostabilumu, monoeksponentine gesimo kinetika ir aukštu ekstinkcijos koeficientu. Tačiau didžiausias jų trūkumas yra sugertis ir fluorescencija žalioje spektro dalyje. Išsamesniam biologinių mėginių vaizdinimui reikalingi raudonai šviečiantys jutikliai.

Pagrindinis šio darbo tikslas – charakterizuoti naujus BODIPY grupe paremtus fluorescencinius molekulinius rotorius ir išsiaiškinti, kokią įtaką jų spektroskopinėms savybėms bei jautrumui aplinkos fizikinėms savybėms turi molekulinės struktūros pokyčiai. Spektroskopinės FMR savybės buvo charakterizuotos naudojant absorbcijos ir fluorescencijos emisijos spektrus bei fluorescencijos gesimo kinetiką. Taip pat buvo ištirta priklausomybė nuo tirpiklio klampos, poliškumo ir temperatūros.

Iš gautų rezultatų galima teigti, kad praplėtus konjuguotą sistemą molekulėse, įvyksta batochrominis poslinkis jų absorbcijos ir fluorescencijos spektruose. Taip pat buvo pastebėta, kad nitro grupės prijungimas padidina fluoroforų jautrumą klampai. Trys nauji mikroklampos jutikliai (BP-Vinyl-NO_2, BP-Ph-mMethyl-NO_2, BP-Ph-oMethyl-NO_2) buvo sėkmingai ištirti bei buvo nustatyta, kad BP-Vinyl-NO_2 molekulė gali būti naudojama, kaip jutiklis ypač klampioms terpėms analizuoti.

SUMMARY

VILNIUS UNIVERSITY
FACULTY OF CHEMISTRY AND GEOSCIENCES

RUGILĖ ŽILĖNAITĖ

Spectroscopic Characterisation of new Fluorescent Viscosity Sensors Based on BODIPY Group

Viscosity plays a significant role on microscopic level in biosystems. It can determine the rate of diffusion-controlled processes, mass transport and intercellular molecular interactions. Atypical changes of intracellular microviscosity are associated with the development of diseases or pathologies. Thus, it is very important to monitor its variations within the cell. One of the most convenient methods to do that is by using viscosity-sensitive fluorophores, called fluorescent molecular rotors (FMRs). After FMR excitation intramolecular rotation occurs, which is dependent on the viscosity of the surroundings. Intramolecular rotation is fast in low viscosity solvents, which leads to an increased non-radiative relaxation, while in high viscosity solvents rotation is slow and fluorescence intensity, thus, increases. Besides the fluorescence intensity, quantum yield and decay time also increases.

Boron-dipyrromethene (BODIPY) based FMRs are widely used as viscosity sensors. In between them, BODIPY-C_{10} and its other derivatives are the most popular molecular rotors. Their main advantages are easy functionalisation, photostability, monoexponential decay and relatively high molar extinction coefficient. However, their main drawback is absorption and fluorescence wavelengths. The most of the BODIPY based probes emit photons in a green spectral region. Red or near-infrared light is more desirable to obtain deeper tissue penetration and minimise light scattering when working with the biological samples.

The main focus of this work is to characterise new BODIPY-based fluorescent molecular rotors and assess how changes in the molecular structure can influence their spectroscopic properties as well as sensitivity to the physical properties of a medium. Absorption and fluorescence emission spectra and fluorescence decays have been recorded to characterise spectroscopic properties of the samples. Dependences on polarity, viscosity, and temperature of the solvent were measured.

The obtained results show that extension of the conjugated system in fluorophores results in a bathochromic shift of both absorption and fluorescence spectra. Moreover, it was found that addition of nitro group enhances viscosity sensitivity of fluorophores. Three new microviscosity probes (BP-Vinyl-NO_2, BP-Ph-mMethyl-NO_2, BP-Ph-oMethyl-NO_2) were successfully investigated. Furthermore, it was shown that BP-Vinyl-NO_2 fluorophore could be used to probe high microviscosity environments.